DOKUZ EYLÜL UNIVERSITY
GRADUATE SCHOOL OF NATURAL AND APPLIED SCIENCES

ANALYTICAL INVESTIGATION OF CORBELS MADE OF ULTRA HIGH PERFORMANCE CONCRETE IN PRECAST REINFORCED CONCRETE STRUCTURES

by

Abdulrahman Shabaan Moshref Mo ELZAINY

December, 2024

İZMİR

ANALYTICAL INVESTIGATION OF CORBELS MADE OF ULTRA HIGH PERFORMANCE CONCRETE IN PRECAST REINFORCED CONCRETE STRUCTURES

A Thesis Submitted to the
Graduate School of Natural and Applied Sciences of Dokuz Eylül University
In Partial Fulfillment of the Requirements for Master of Science in
Department of Civil Engineering, Structural Engineering Program

by

Abdulrahman Shabaan Moshref Mo ELZAINY

December,2024

İZMİR

THESIS EXAMINATION RESULT FORM

We have read the thesis entitled **"ANALYTICAL INVESTIGATION OF CORBELS MADE OF ULTRA HIGH PERFORMANCE CONCRETE IN PRECAST REINFORCED CONCRETE STRUCTURES"** completed by **ABDULRAHMAN SHABAAN MOSHREF MO ELZAINY** under supervision of **ASSOC.PROF.DR. SADIK CAN GİRGİN** and **ASSOC.PROF.DR. ÇAĞLAR YALÇINKAYA** and we certify that in our opinion it is fully adequate, in scope and in quality, as a thesis for the degree of.Master of Science.

Asst.Prof.Dr. Sadık Can GİRGİN

Supervisor

Prof. Dr. Özgür ÖZÇELİK

Jury Member

Assoc. Prof.Dr. Selçuk SAATCI

Jury Member

Prof. Dr. Abdullah SEÇGİN

Director

Graduate School of Natural and Applied Sciences

ACKNOWLEDGMENT

First and foremost, many thanks go to my advisors, Assoc. Prof. Dr. Sadık Can Girgin and Assoc. Prof. Dr. Çağlar Yalçınkaya, for advising, teaching, and encouraging me along this wonderful and life-changing journey. I have learned a great deal from them, and I'm truly grateful.

I would also like to thank Prof. Koutromanos for providing the FE-MultiPhys program and the resources needed to complete this study.

Finally, thanks to my family for their constant support and always keeping me focused. If not for them, I wouldn't be where I am today, and I'm grateful for all the care and guidance they've given me.

Abdulrahman Shabaan Moshref Mo ELZAINY

ANALYTICAL INVESTIGATION OF CORBELS MADE OF ULTRA HIGH PERFORMANCE CONCRETE IN PRECAST CONCRETE STRUCTURES

ABSTRACT

Concrete corbels in precast concrete structures are critical in transferring vertical and horizontal loads from beams to columns or walls, often under complex stress conditions. Therefore, their design must ensure safe load transmission without failure or significant plastic deformation. While traditional corbels made of Normal Strength Concrete (NSC) have been extensively studied, they exhibit limitations such as increased weight, honeycomb formations, and low force-displacement capacity. The use of Ultra-High-Performance Concrete (UHPC) offers a promising alternative, significantly enhancing the structural performance of corbels by improving their force-displacement capacity, ductility, and durability, thanks to UHPC's exceptional mechanical properties. However, as a relatively new material, UHPC lacks sufficient experimental data in the literature, and existing material models in Finite Element (FE) analysis software often fail to predict its behavior accurately.

This study involved a numerical analysis of UHPC corbels by calibrating an existing material model in the LS-DYNA finite element software and implementing a triaxial constitutive concrete model proposed by Moharrami and Koutromanos (2016) within the FEMultiphys software. Furthermore, a strut-and-tie model developed specifically for UHPC corbels was implemented to calculate their ultimate capacity. The results from these different models are compared with experimental data to assess the reliability of these analytical methods.

Keywords: Precast concrete structures, corbels, ultra-high-performance concrete, finite element analysis

ÖNÜRETİMLİ BETONARME YAPILARDA ULTRA YÜKSEK PERFORMANSLI BETONDAN YAPILAN KISA KONSOLLARIN ANALİTİK OLARAK İNCELENMESİ

ÖZ

Ön üretimli betonarme yapılardaki beton konsollar, karmaşık gerilme koşulları altında genellikle kirişlerden kolonlara veya duvarlara dikey ve yatay yüklerin aktarılmasında kritik bir rol oynar. Bu nedenle, tasarımlarının, arızalanma veya önemli plastik deformasyon olmaksızın güvenli yük aktarımını sağlaması gerekmektedir. Normal Dayanımlı Beton (NDB) kullanılarak yapılan geleneksel konsollar geniş çapta incelenmiş olmasına rağmen, bu tür konsollar artan ağırlık, boşluklu yüzey oluşumu ve düşük kuvvet-yer değiştirme kapasitesi gibi sınırlamalar sergiler. Ultra Yüksek Performanslı Beton (UYPB) kullanımı, UHPC'nin olağanüstü mekanik özellikleri sayesinde kuvvet-yer değiştirme kapasitesini, sünekliğini ve dayanıklılığını artırarak konsolların yapısal performansını önemli ölçüde iyileştiren umut verici bir alternatif sunmaktadır. Bununla birlikte, nispeten yeni bir malzeme olan UYPB, literatürde yeterli deneysel veriye sahip değildir ve Sonlu Elemanlar (FE) analiz yazılımlarındaki mevcut malzeme modelleri genellikle bu malzemenin davranışını doğru şekilde tahmin edememektedir.

Bu çalışma, LS-DYNA sonlu eleman yazılımındaki mevcut bir malzeme modelinin kalibrasyonu ve Moharrami ve Koutromanos (2016) tarafından önerilen üç eksenli bir beton modelinin FEMultiphys yazılımında uygulanması yoluyla UHPC konsolların sayısal analizini içermektedir. Ayrıca, UHPC konsollar için özel olarak geliştirilen bir çubuk ve düğüm modeli nihai kapasitesini hesaplamak için uygulanmıştır. Farklı modellerden elde edilen sonuçlar, bu analitik yöntemlerin güvenilirliğini değerlendirmek amacıyla deneysel verilerle karşılaştırılmıştır.

Anahtar kelimeler: Önüretimli betonarme yapılar, kısa konsollar, ultra yüksek performanslı beton (UYPB), sonlu elemanlar analizi

CONTENTS

Page

LIST OF FIGURES

Page

LIST OF TABLES

Page

CHAPTER ONE
INTRODUCTION

Precast concrete technology has gained increasing attention in the construction industry in recent decades and is considered a reliable and effective alternative to the typical cast-in-situ methods. The precast concrete elements are fabricated in a controlled environment and then relocated to the construction site for assembly. The advantages of precast concrete structures, like the high-quality concrete elements, less environmental impact, and reduced construction time, assure more efficient and durable structures. Precast concrete technology has made constructing various structures easier, from commercial buildings to industrial facilities and bridges. One of the essential structural elements in precast concrete structures (e.g., bridges) is corbels, which typically project from the side faces of columns. Corbels serve an essential role, transmitting vertical and horizontal loads from beams or slabs to columns while ensuring the stability and integrity of the structure. Many parameters should be considered when designing a concrete corbel, including shear span-to-depth ratio, main and secondary reinforcement amount, and material characteristics. Therefore, considering any possible performance-affecting factor during the design phase, providing safe corbels that can support service loads with minimal crack widths and plastic deformation is mandatory. The research conducted in the last decades has come a long way regarding corbels designed using traditional materials like Normal Strength Concrete (NSC). Current design codes and standards have established reliable and safe design methods for conventional concrete corbels. However, NSC corbels impose several limitations, including dense reinforcement, increased corbel weight, low load-displacement capacity, and low ductility, which heavily impact the overall performance of the concrete structure.

Enhancing the structural performance of corbels can be done in many ways. One of the most influential factors is changing the materials used to make corbels—efforts to enhance concrete succeeded by adding other materials or changing its composition. One of the most effective additions to concrete is fiber, which noticeably enhances the mechanical properties of concrete (e.g., ductility) when added. Ultra-high-performance concrete (UHPC) is one product of this extensive research on concrete,

which was proven in many studies to attain exceptional mechanical properties better than that of the NSC (e.g., durability, ductility, and low porosity) with higher compressive strength ranging from 120 MPa to 200 MPa. It was proven in previous studies that the use of UHPC instead of NSC enhances the performance of structural elements. According to Elzainy et al. (2023), a numerical investigation concluded that the use of UHPC in a hybrid column increases the force-displacement capacity of the column. Research to establish material models to capture the behavior of concrete materials has gone a long way over the last two decades. It has led to the development of a wide range of material models that can successfully analyze and predict the behavior of NSC. However, while experiments on UHPC are still carried on, numerically investigating UHPC is still a challenging task because most available material models are developed based on NSC research data, which means that these material models are unsuitable to be used to analyze UHPC with acceptable accuracy.

While developing an entirely new material model specifically for UHPC needs extensive experimental and analytical investigation, this study proposes a reliable alternative by utilizing and calibrating existing material models. Two material models were utilized in this study. The first one is the Karagozian and Case Concrete material model (K&C) (Malvar et al., 1997), found in the finite element software LS-DYNA. The second one, the Triaxial Constitutive Model proposed by Moharrami and Koutromanos, (2016), is available in the finite element software package FEMultiPhys. Several parameters in the K&C material model were calibrated to predict the softening behavior of UHPC. The material model was calibrated using a constitutive concrete model proposed by Zhang et al. (2023), which considers fibers effect. The test result from Xu & Wille, (2014) was used to validate the outcome of the constitutive model. The calibrated model was validated using a single-element model, and the result was compared with the experimental data. Furthermore, a direct tensile test data was used to calibrate the tensile softening and fiber reinforcement parameters of the Triaxial Constitutive Model proposed by Moharrami and Koutromanos, (2016). Additionally, a modified strut-and-tie model developed by Huang et al. (2024), which considers the fiber reinforcement forces while designing corbels made of UHPC, is used since the traditional strut-and-tie model cannot consider the fiber reinforcement effect while designing D-region sections. The results

obtained from the FE analysis and the modified strut-and-tie model were compared to assess the accuracy of the analytical models.

CHAPTER TWO
LITERATURE REVIEW

2.1 Introduction

Although existing material models are suitable to analyze NSC, they cannot be used with UHPC due to the difference between NSC and UHPC. For instance, there is an unneglectable difference between NSC and UHPC regarding strain-hardening behavior. Therefore, a different material model must be used to capture the UHPC behavior. However, extensive experimental investigation is required to develop a new material model. calibrating the existing material models is another approach. A literature review of the K&C material model, the Triaxial constitutive model, and the modified strut-and-tie model is presented in this chapter.

2.2 Ultra-High-Performance Concrete (UHPC)

UHPC is a new type of NSC developed by the U.S. Army Engineering Research and Development Center in the early 1980s for military purposes (Green et al., 2014). Other countries have started experimenting with UHPC for civil applications. For instance, the first UHPC roadway was built in France, while UHPC field construction began in 2006 in the U.S. (Tadros et al., 2020). UHPC has exceptional mechanical characteristics like high strength, durability, and ductility. The UHPC has several characteristics, including a tensile strength of more than 5 MPa, a compressive strength exceeding 120 MPa, and high ductility (Kravanja et al., 2024). The use of fine aggregates (>5 mm), micro silica, superplasticizers, and fiber reinforcement significantly increases the shear and flexure strength of UHPC and, as a result, enhances the ductility of UHPC (Shekarchi et al., 2020). It was also proven that the dense microstructure and low porosity of the UHPC greatly enhance the bond performance (Feng et al., 2020). The porosity of the cementitious material heavily affects the durability of Reinforced Concrete (RC) structures. Research shows that RC structures made of NSC have less service life because NSC is more porous, which helps initiate steel corrosion faster, especially in the areas where either carbon dioxide

concentration is high or the conditions of humidity (40%-80%) and temperature (20-50°C) or both are encountered. On the other hand, the dense microstructures of UHPC significantly delay the initiation of steel corrosion, increasing the durability and the service life of RC structures (Sohail et al., 2021). Additionally, UHPC, unlike NSC, does not immediately fracture after reaching its' tensile strength, as shown in Figure. 2.1. UHPC exhibits ductility after reaching first-crack stress, where multiple cracks accumulate within the specimen. However, the crack-bridging effect induced by fibers in UHPC keeps the concrete member from fracturing immediately. After that, the cracks concentrate in one big crack until reaching a threshold value known as the tensile fracture energy, where this single big crack widens until complete failure (Gee et al., 2020).

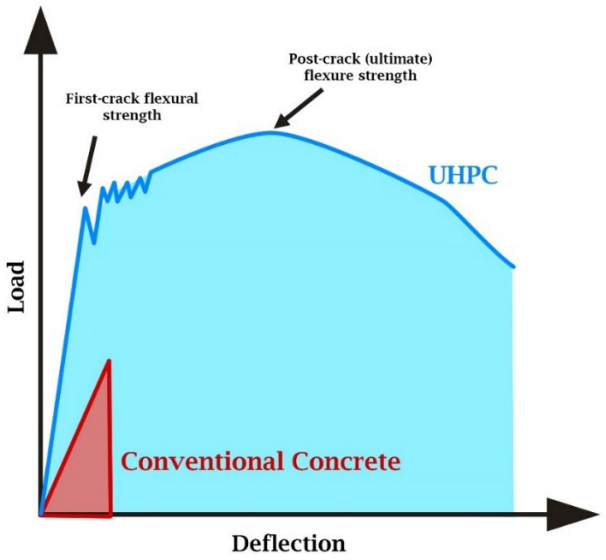

Figure 2.1 Comparison between UHPC and NSC in terms of load-deflection

In an experimental study by Ridha et al. (2017), the shear-span to-depth ratio, main reinforcement ratio, and secondary reinforcement ratio of eleven UHPC corbels subjected to monotonically increasing load were investigated to monitor their effect on the shear capacity and failure mode of the corbels. The test results demonstrated the effectiveness of corbels made of UHPC with steel fibers.

2.3 The Karagozian and Case Concrete Material Model

The Karagozian and Case (K&C) model is a material model available in the finite element software LS-DYNA capable of modeling concrete behavior under various loading conditions Wu & Crawford, (2015). The K&C material model was first developed in 1994, utilizing excellent capabilities, such as three independent failure surfaces, as shown in Figure. 2.2. introducing strain rate enhancement algorithm and considering fracture energy's effect under tension (Malvar et al., 1997). The current K&C version is the third release under the name *MAT_CONCRETE_DAMAGE_REL3 in LS-DYNA. This material model has several enhanced characteristics, such as reduced mesh dependencies and the generation of all the concrete parameters using the unconfined compressive strength only (Magallanes et al., 2010). The recent improvements introduced to the K&C material model allowed researchers to investigate elastic hardening degradation for cyclic loading and the effect of strain rate on viscoelastic flow (Abakumov et al. 2023).

The K&C requires calibration when used with other materials. Multiple researchers calibrated the K&C material model parameters to analyze different materials. For example, the K&C model was modified to investigate the dolomite rock, and the result shows a good agreement with the experimental data (Kucewicz et al., 2020). The fiber-reinforced concrete was analyzed using a calibrated version of the K&C (Thai & Nguyen, 2020) and strain-hardening fiber-reinforced cementitious composites (Yin et al. 2022). Various tests like impact and explosion were used to validate the calibrated material model in dynamic testing schemes and uniaxial and triaxial compression tests (Yin et al., 2022; Kucewicz et al., 2020). Xu & Wille (2014) used constitutive models to calibrate the K&C material model for UHPC, while the machine-learning capabilities were implemented in recent research to calibrate the K&C material model parameters for Fiber Reinforced Concrete (FRC) and UHPC (Yaşayanlar, 2023).

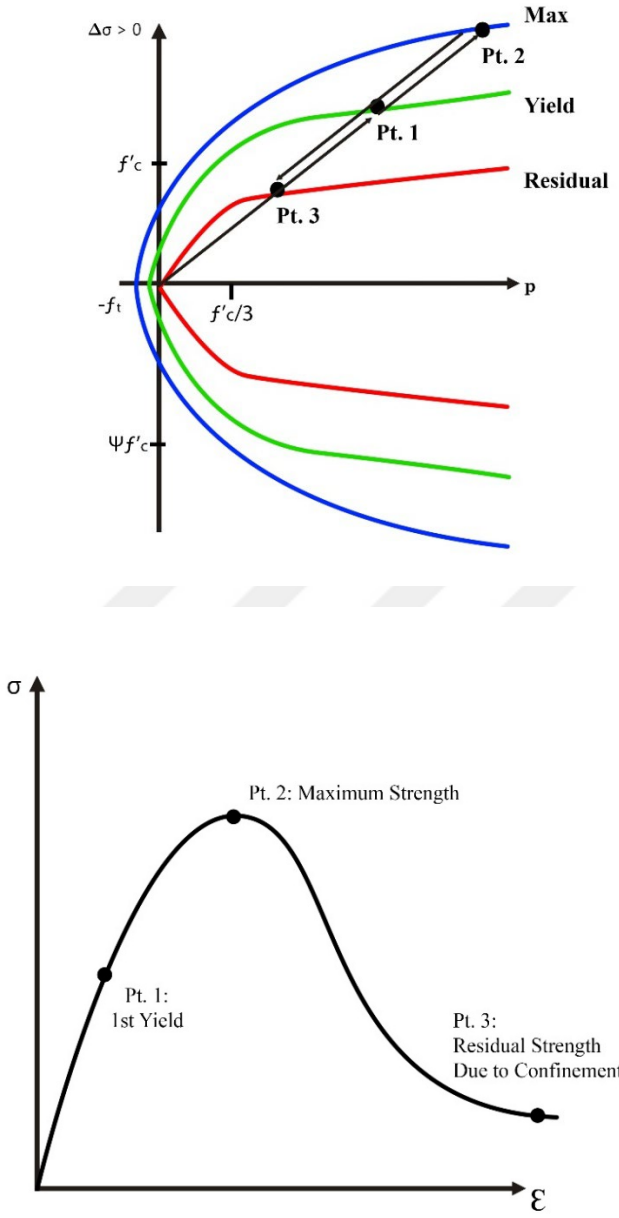

Figure 2.2 K&C three failure surfaces (Malvar et al. 1997).

2.4 The Triaxial Constitutive Model (Moharrami and Koutromanos, 2016)

The Triaxial Constitutive Model is a material model Moharrami and Koutromanos (2016) proposed, utilizing elastoplastic formulation, a nonassociative flow rule, and a rotating smeared-crack model. The triaxial material model captures the cracking behavior of concrete and the confining effect during analysis, making it a suitable model to investigate NSC and FRC materials. For instance, He et al. (2021)

investigated the cracking behavior of concrete under cyclic loading using the material model proposed by Moharrami and Koutromanos, (2016). The triaxial material model was also used by Fawaz & Murcia-Delso (2021) to consider the low-cycle fatigue and bond slip of reinforcement to predict the cyclic response of RC columns.

The material model proposed by Moharrami and Koutromanos (2016) has been recently investigated and modified to analyze fiber-reinforced cementitious materials. The material model is now capable of capturing the crack-bridging effect induced by fibers, and fiber orientation is also taken into consideration during analysis by simplifying their orientation into three main directions, as seen in Figure 2.3, which has been proven to affect the analysis result significantly (El-Helou et al., 2020).

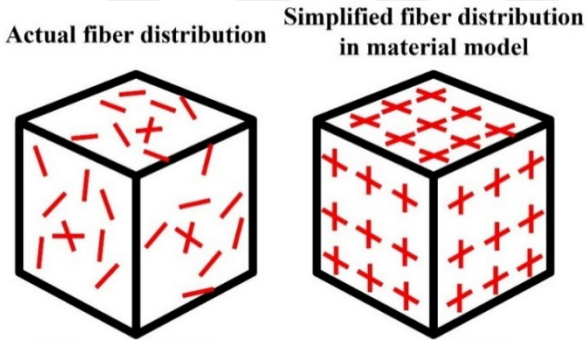

Figure 2.3 Simplified fiber orientation in the material model by Moharrami and Koutromanos, (2016).

2.5 The Strut-and-Tie model

One of the effective approaches to designing RC members undergoing a complex stress state known as the D-region sections is the Strut-and-Tie model (STM) (Panjehpour et al., 2012). The STM usually comprises compression struts, tension ties, and nodes, which represent the flow of stresses within the structural member—the primary purpose of the STM is to investigate the safety of structural members designed with different materials. Although the STM is an excellent designing tool, it can be challenging to determine the factors of struts' effectiveness, strain compatibility, and anchorage requirements (Panjehpour et al., 2012). The STM has been further optimized to include the design of three-dimensional structures (Leu et al., 2006). Various structural members can be designed using the STM like corbels, deep beams, and beam-column joints, as shown in Figure 2.4 (Zhang et al., 2020; He et al., 2013).

Traditional STM used to design structural members made of NSC cannot be used with other materials like UHPC, and modification of the STM is required. Kassem (2015) further modified the STM using laws of cracked reinforced concrete and strain compatibility, and the accuracy of ultimate load prediction was acceptable. In another research, the contribution of reinforcement forces was considered, and the proposed modified STM successfully predicted the ultimate capacity of UHPC corbels (Al-Quraishi et al., 2018).

Huang et al. (2024) experimented on twelve UHPC corbels subjected to monotonic load, investigating several parameters, including the shear span-depth ratio and steel fiber volume. The study shows that corbels reinforced with steel fibers have significantly higher cracking loads than those without steel fibers. Corbels with steel fiber reinforcement experience flexure failure mode. Furthermore, it has been proven that the shear capacity of UHPC corbels improves when secondary reinforcement is introduced. Finally, a modified STM based on the truss method was proposed, considering main reinforcement, secondary reinforcement, and fiber forces. The proposed STM's accuracy was validated and proven superior to the current STM (Huang et al., 2024).

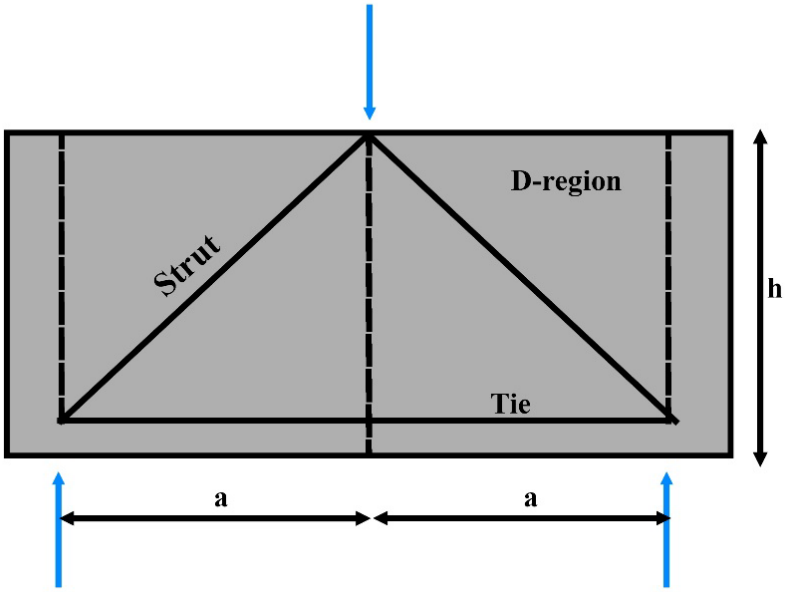

(a)

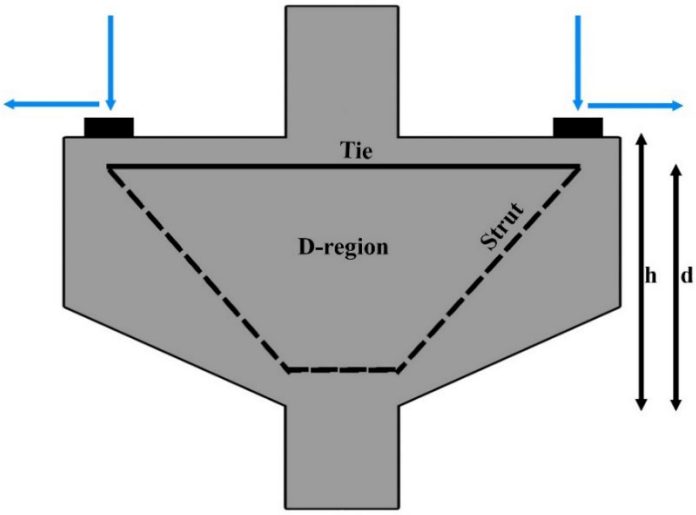

(b)

Figure 2.4 Examples of D-region elements. (a) Deep beam, (b) Corbel.

CHAPTER THREE
CALIBRATION OF THE KARAGOZIAN AND CASE MATERIAL MODEL

3.1 Introduction

This chapter presents the Karagozian and Case (K&C) concrete material model in detail. Researchers have proposed several calibration procedures for the K&C material model. For instance, Yaşayanlar (2023) utilized a Deep Neural Network scheme to calibrate the K&C material model for Fiber Reinforced Concrete (FRC) and Ultra High-performance Concrete (UHPC).

A constitutive model by Zhang et al. (2023) and uniaxial compression test data of UHPC specimens were used side by side to calibrate the K&C material model in this study.

3.2 Methodology

The finite element software LS-DYNA enabled researchers and engineers to investigate members using linear and nonlinear analysis and to use a wide range of material models under various loading cases. The K&C is one of these material models that can capture various materials' behavior under static and dynamic events. For instance, the K&C material model was utilized to capture the behavior of high-performance fiber-reinforced cement composite (HPFRCC) (Lee & Park, 2023), fiber-reinforced concrete (FRC) (Nguyen et al., 2021), dolomite rock (Kucewicz et al., 2020), and asphalt concrete (Wu et al., 2017), several loading schemes like blast, high strain rates, and low-velocity impact.

The K&C material model consists of various parameters that describe different aspects of concrete behavior. The current version of the K&C material model can generate material parameters for Normal Strength Concrete (NSC) using the unconfined compressive strength of concrete and reducing the mesh dependencies due to strain-softening (Magallanes et al., 2010). However, using the K&C material model

to analyze any material that has a different behavior than NSC will not yield accurate results since the auto-generated parameters are based on the experimental data conducted on NSC, and a calibration of the K&C material model is needed. A comparison between a test specimen from Xu & Wille (2014) and the analysis result using the K&C model with auto-generated parameters is shown in Figure 3.1, proving that the current state of the K&C material model is unsuitable for UHPC analysis.

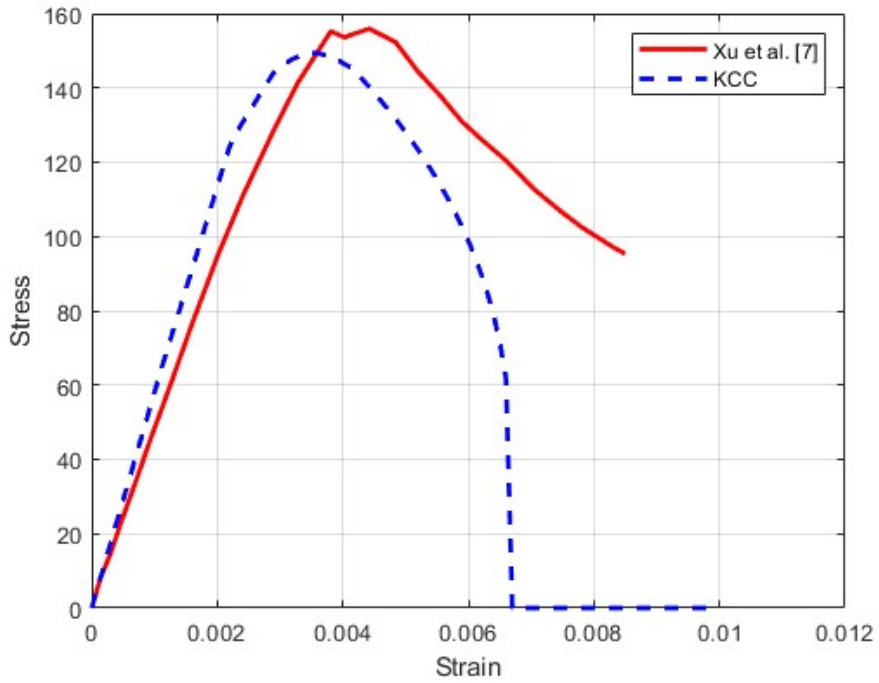

Figure 3.1 Comparison between uniaxial test data and the KCC model with auto-generated parameters

Recent research proposed various calibration procedures for the K&C material model. While the calibration of the K&C material model requires uniaxial and multiaxial test data, this study follows an easy and effective approach outlined in Man Xu & Wille (2014), where a constitutive model has been utilized to obtain the uniaxial and triaxial data.

An essential step in the calibration procedure is implementing a suitable constitutive model to obtain the corresponding parameters for UHPC. There are several empirical models proposed for concrete in the literature, like Drucker and Prager's (1957) model, Malvar et al. (1997) model, Mander et al. (1988) model, and Saatcioglu and Razvi (1992) model. etc. However, these constitutive models are not used since they are

based on NSC test data. Therefore, a constitutive model that has been developed explicitly for UHPC/UHPFRC by Zhang et al. (2023) is utilized in this study.

The validity of the constitutive model is first assessed by comparing its output with the available experimental results. The data obtained from the constitutive model is used to calibrate the parameters of the K&C model. The calibrated material model is then applied to a partially fixed hexahedral single-element model that is partially fixed and uniaxially compressed. The analytical results are compared to the constitutive model for validation.

3.3 The calibration procedure of the K&C material model for UHPC

The calibration of the K&C material model starts by obtaining the uniaxial and triaxial data using the proposed constitutive model by Zhang et al. (2023). This model is utilized to calibrate the failure surface parameters (yield, maximum, and residual surface), the equation of state, and the damage function. This section presents the detailed calibration procedure of the K&C material model.

3.3.1 Determination of the uniaxial and triaxial data

To appropriately calibrate the K&C material model, uniaxial and triaxial test data must be obtained. An empirical model proposed by Zhang et al. (2023) is used in this study to determine the stress-strain curve for UHPC with 150 MPa as the unconfined compressive strength and 2% steel fiber under different confinement stresses (5, 10, and 20 MPa).

Equation (3.1) from Popovics, (1973), which is used by many researchers, such as Xiao et al. (2010), Candappa et al. (2001), and Mirmiran et al. (1997), to obtain the ascending portion of the axial stress-strain data for NSC and High-Strength Concrete (HSC), is adopted in this study.

$$\frac{\sigma_c}{f_{cc}} = \frac{\left(\frac{\varepsilon_c}{\varepsilon_{cc}}\right) \times r}{r - 1 + \left(\frac{\varepsilon_c}{\varepsilon_{cc}}\right)^r} \tag{3.1}$$

$$r = \frac{E_c}{E_c + \frac{f_{cc}}{\varepsilon_{cc}}} \tag{3.2}$$

Where σ_c and ε_c are axial stress and axial strain, f_{cc} and ε_{cc} are the maximum axial stress and corresponding axial strain, respectively, and E_c is the elastic modulus, which according to Teng et al. (2019) can be obtained from equation (3.3).

$$E_c = 35497.50 + 78.00 \times f'_{co} \tag{3.3}$$

Where f'_{co} is UHPC unconfined compressive strength.

The descending portion of the curve can be calculated from equations (3.4-3.5).

$$\sigma_c = f_{cres} + \frac{f_{cc} - f_{cres}}{1 + n \times \left(\frac{\varepsilon_c}{\varepsilon_{cc}} - 1\right)^2} \tag{3.4}$$

$$n = \frac{2}{1+100V_{sf}} \tag{3.5}$$

Where V_{sf} is the percentage of steel fiber and n is the factor that describes the effect of steel fibers on the stress-strain relationship for the post peak descending portion of the stress-strain curve.

The axial residual stress f_{cres} is a critical parameter that must be obtained to complete the entire stress-strain curve and to calibrate the K&C model failure surface parameters. It has been proven in various studies to exist after the descending portion of the stress-strain curve for concrete subjected to triaxial compression (Attard et al. 1996, Xie et al. 1995, and Binici, 2005). The axial residual stress of UHPC increases

with the increase of the hydraulic pressure, as seen from test results by Zhang et al. (2023). The definition of axial residual stress differs in various studies. For instance, Xie et al. (1995) have taken the axial residual stress as the point where the remaining portion of the descending curve is less than 2% than the initial ascending curve. Samani and Attard (2012) found that the endpoint of the axial stress-strain curve represented the closest value of the axial residual stress reported in various tests. Smith et al. (1989) described the axial residual stress as the axial stress corresponding to the lateral strain of 0.03. However, it was proven by Zhang et al. (2023) that this method is inaccurate with specimens with long post-peak descending curves. In this study, the method followed by Xie et al. (1995) is adopted, and the axial residual stress is calculated using the linear equation (3.6) proposed by Zhang et al. (2023).

$$\frac{f_{cres}}{f'_{co}} = 9V_{sf} + 4.7 \times \left(\frac{f_l}{f'_{co}}\right) \tag{3.6}$$

Where f_l is the confining pressure.

While the peak axial stress f_{cc} of UHPC increases with the increase of the confining pressure f_l like NSC and HSC, it was seen that the enhancement of the axial stress is slightly reduced with the addition of steel fibers (Wang et al. 2020 and Zhang et al. 2023). The peak axial stress f_{cc} and corresponding axial ε_{cc} strain is calculated using the proposed equations (3.7-3.8) by Zhang et al. (2023).

$$\frac{f_{cc}}{f'_{co}} = 1 + (3.1 - 16V_{sf}) \times \left(\frac{f_l}{f'_{co}}\right)^{0.7} \tag{3.7}$$

$$\frac{\varepsilon_{cc}}{\varepsilon_{c0}} = 1 + (12 + 100V_{sf}) \times \left(\frac{f_l}{f'_{co}}\right)^{1.5} \tag{3.8}$$

Where ε_{c0} is taken as 0.435% For UHPC with 150 MPa as the unconfined compressive strength according to Zhang et al. (2023).

The axial strain-lateral strain relationship describing the UHPC dilation behavior under different confining pressures is calculated using the modified equation (3.9) by Zhang et al. (2023).

$$\frac{\varepsilon_c}{\varepsilon_{c0}} = \left(1 + 4.3\left(\frac{f_l}{f'_{co}}\right)^{0.9}\right) \times \left\{\left[1 + 0.53\left(-\frac{\varepsilon_l}{\varepsilon_{c0}}\right)\right]^{(f)} - \exp\left[-7\left(-\frac{\varepsilon_l}{\varepsilon_{c0}}\right)\right]\right\} \quad (3.9)$$

$$f = 0.58 \times \left(\frac{f_l}{f'_{co}}\right)^{(0.1+0.5V_{sf})} + 0.3 \quad (3.10)$$

Where f is the function representing the confinement ratio $\left(\frac{f_l}{f'_{co}}\right)$.

By utilizing equations (1-10), the stress-strain curves for UHPC with 150 MPa unconfined compressive strength and 2% fiber volume are obtained under three levels of confinement (5, 10, 20) as shown in Figure 3.2.

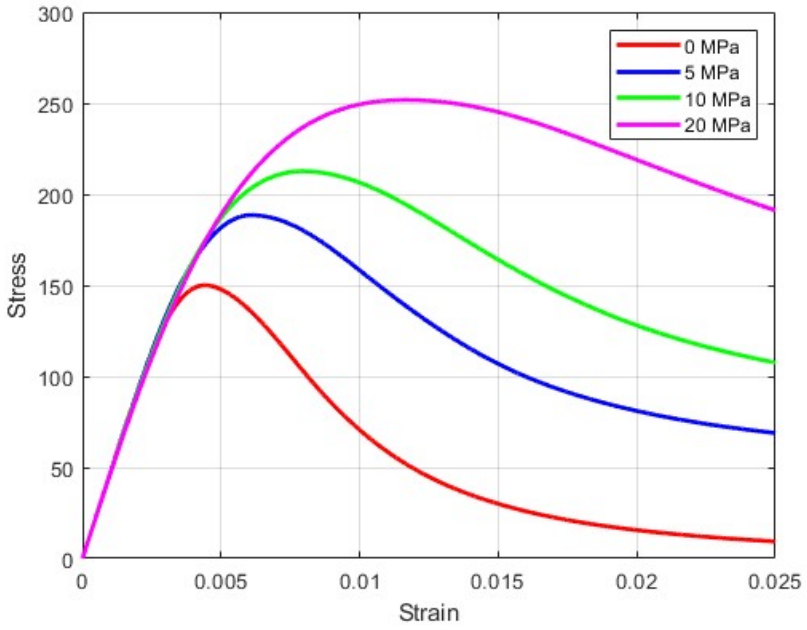

Figure 3.2 UHPC stress-strain curves under different confinement levels

To ensure that the output taken from the constitutive model proposed by Zhang et al. (2023) is suitable for calibrating the K&C material model, the uniaxial compression result is plotted against a specimen test result from Xu & Wille (2014) in Figure 3.3. The comparison shows a good agreement with the test data, meaning that the uniaxial and triaxial data taken from the constitutive model can calibrate the K&C parameters.

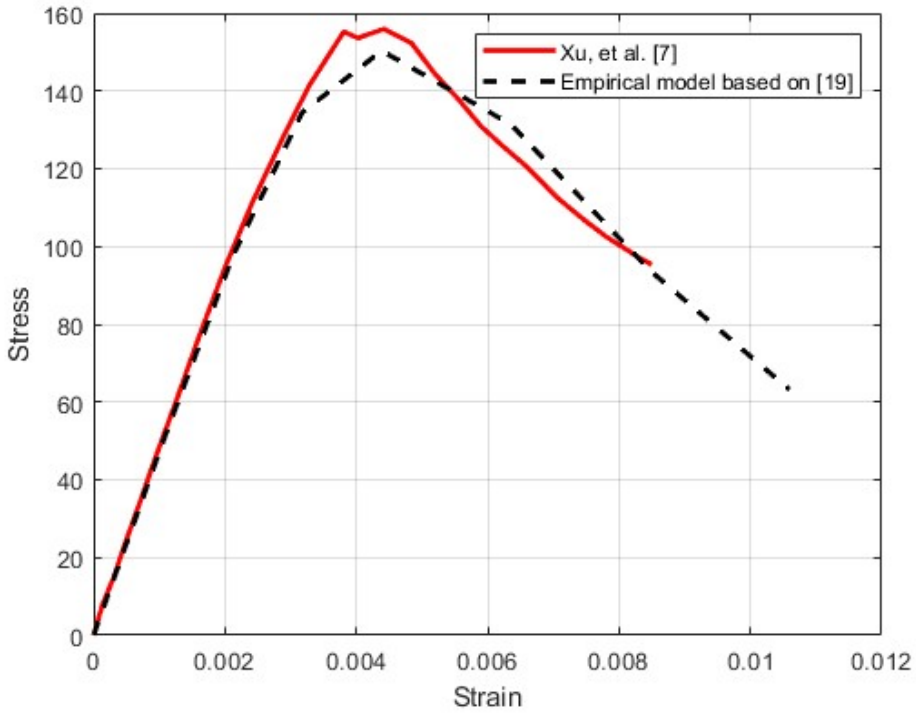

Figure 3.3 Comparison between uniaxial test data from Xu & Wille, (2014) and Zhang's empirical model.

3.3.2 Calibrating the K&C failure surfaces

The K&C material model utilizes three failure surfaces, each defining the behavior of concrete at three different stages.

The first failure surface is the yield failure surface, which represents the initial yielding in the K&C material model, and it is represented by the three parameters α_{0y}, α_{1y}, and α_{2y} (Malvar et al., 1997). The yield failure surface is defined by the equation (3.11).

$$\Delta\sigma_y = \alpha_{0y} + \frac{p}{\alpha_{1y} + \alpha_{2y}p} \tag{3.11}$$

The second failure surface is the maximum failure surface, representing the strain hardening of the concrete material. This surface defines the transition in behavior from the linear stage to the nonlinear stage up to the maximum strength of concrete. The

maximum failure surface is described by the three parameters α_0, α_1, and α_2 in the equation (3.12).

$$\Delta\sigma_m = \alpha_0 + \frac{p}{\alpha_1 + \alpha_2 p} \tag{3.12}$$

The third and final failure surface is the residual failure surface marking the end point after which the strain softening occurs in the K&C material model and it is established using the two parameters α_{1f} and α_{2f}, which is depicted in equation (3.13).

$$\Delta\sigma_r = \frac{p}{\alpha_{1f} + \alpha_{2f} p} \tag{3.13}$$

Where p and $\Delta\sigma$ are the stress difference and mean stress respectively, and they are represented by the equations (3.14-3.15).

$$p = \frac{1}{3}(\sigma_1 + \sigma_2 + \sigma_3) \tag{3.14}$$

$$\Delta\sigma = \sqrt{\frac{(\sigma_1 - \sigma_2)^2 + (\sigma_1 - \sigma_3)^2 + (\sigma_3 - \sigma_2)^2}{2}} \tag{3.15}$$

Where σ_1, σ_2, and σ_3 are the axial stress at each shear failure surface (yield, maximum, and residual) and the corresponding lateral confining pressures respectively.

The UHPC meridian plane must be plotted for each level of confinement to determine the full set of failure surface parameters. The maximum failure surface σ_m and residual failure surface σ_r are determined from Figure 3.2 and used in equations (3.14 – 3.15) to determine the stress difference and mean stress.

Since UHPC yield strength tests are still lacking, this study implements a method mentioned in Malvar et al. (1994) to calculate the yield failure surface parameters

using the maximum failure surface, which can be obtained from equations (3.16 – 3.17).

$$\Delta\sigma_y = 0.45\Delta\sigma_m \tag{3.16}$$

$$P' = P - 0.55/3\Delta\sigma_m \tag{3.17}$$

Finally, Figure 3.4 plots the meridian plane of the yield, maximum, and residual failure surfaces. Using the obtained meridian plane and equations (3.11-3.13), nonlinear regression calculates the failure surface parameters in Table 3.1.

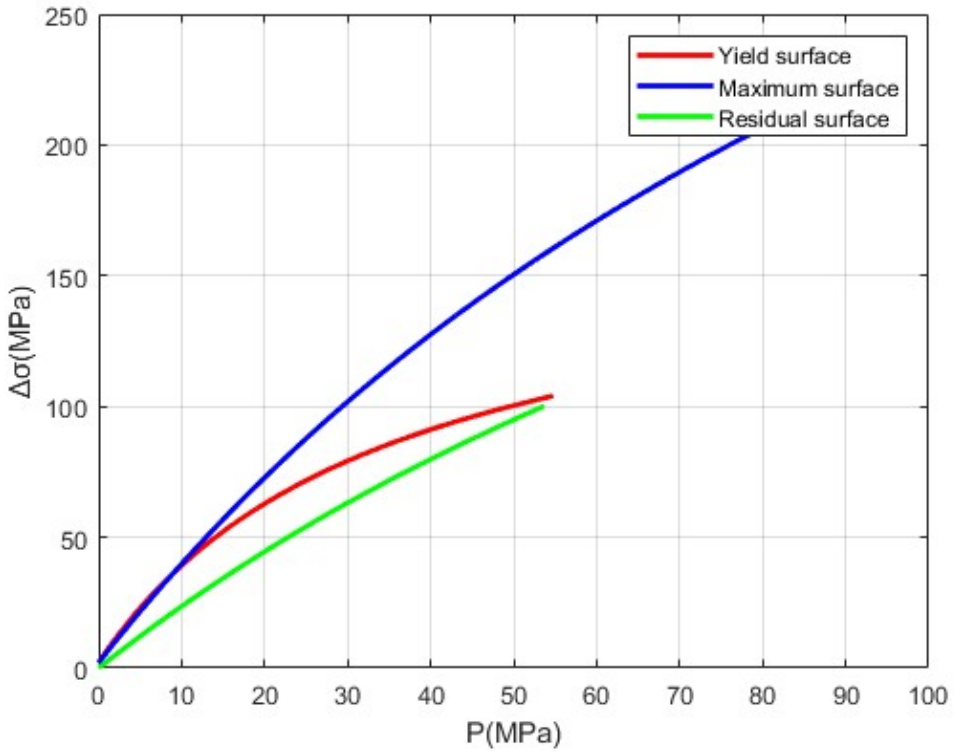

Figure 3.4 Meridian plane.

Table 3.1 The calibrated K&C material model's failure surface parameters.

Parameter	Value
α_0	2.03748
α_1	0.24654
α_2	0.00180
α_{1f}	0.39810
α_{2f}	0.00257
α_{0y}	2.08075
α_{1y}	0.20987
α_{2y}	0.00598

3.3.3 Calibrating the Equation of State (EOS)

The K&C material model implements a tabulated compaction EOS to describe the volumetric behavior of the concrete material under hydrostatic pressure, defined in the keyword *EOS_TABULATED_COMPATION in LS-DYNA. The EoS is defined as:

$$P = C(\mu) + \gamma_0 T(\mu) E_0 \tag{3.18}$$

Where $C(\mu)$, γ_0, E_0, *and* $T(\mu)$ are the tabulated mechanical pressure, specific heat modulus, internal energy, and the temperature tabulated parameter, respectively.

The model incorporates ten pairs of pressure *P* and corresponding volumetric strain μ to derive the EoS, divided into three zones as seen in Figure 3.5: elastic, compaction, and solidification. In the elastic phase, the voids within concrete behave elastically under hydrostatic pressure until they reach the elastic limit. The elastic limit marks the start of the compaction phase, where voids inside the concrete collapse. The solidification phase indicates no more voids within the concrete, which means there will be an increase in pressure with a minimal increase in volumetric strain.

To establish the EoS for UHPC, the elastic limit must be calculated first. This limit is marked by the threshold value $P_{crushing}$ and $\mu_{crushing}$. It has been proven in previous studies that the $P_{crushing}$ increases with the increase in the compressive strength of UHPC (Xu et al., 2020; Erzar et al., 2016, and Williams et al., 2009). Su et al. (2022) established a relationship between $P_{crushing}$ and the unconfined compressive strength of concrete f'_{co} in equation (3.19). The volumetric strain at the end of the elastic stage can be calculated easily using the obtained. The elastic stage can be calculated easily using equation (3.20).

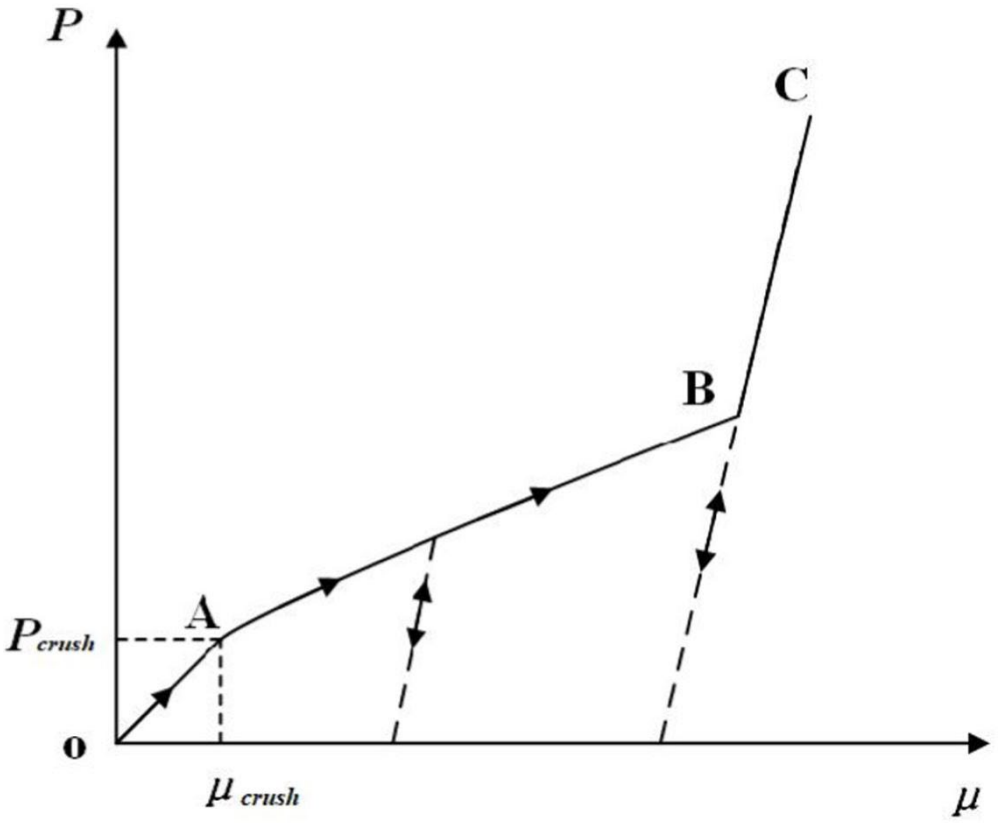

Figure 3.5 EOS of concrete (Su et al. 2022)

$$P_{crushing} = 1.325f'_{co} - 6.199 \tag{3.19}$$

$$K = \frac{P_{crushing}}{\mu_{crushing}} = \frac{E}{[3(1-2v)]} \tag{3.20}$$

Where K is the bulk modulus and v is the Poisson's ratio, which is recommended to be 0.2 according to Xu et al. (2020).

The inelastic stages of the EOS can be obtained from a third-order polynomial (3.21) proposed by Yasser (2022). The calculated EOS is in Table 3.2.

$$p'(MPa) = 0.004248\mu'^{3} - 0.09273\mu'^{2} + 1.294\mu' - 0.415 \ (P_{crushing} \leq p) \tag{3.21}$$

Where $p' = \frac{p}{P_{crushing}}$ and $\mu' = \frac{\mu}{\mu_{crushing}}$

Table 3.2 The calibrated EOS.

Volumetric strain	Pressure (MPa)
0	0
-0.007379166	192.55
-0.010833655	250.00
-0.015809700	380.00
-0.023088268	550.00
-0.032446001	740.00
-0.101574298	2100.00
-0.129214408	3200.00
-0.150309559	4500.00
-0.163806555	5600.00

3.3.4 Calibrating the damage parameters

The K&C model employs 13 pairs to define the damage function $\eta(\lambda)$, which describes the damage evolution in concrete elements. The parameters defining damage accumulation significantly impact the hardening and softening stages. Since UHPC exhibits different behavior in the hardening and softening stages than that of NSC due to a variety of characteristics such as ductility and the presence of steel fibers, it is

mandatory to calibrate these 13 pairs to accurately capture the behavior of UHPC at the hardening stage between yield failure surface and maximum failure surface and then at the softening stage between maximum failure surface and residual failure surface.

To calibrate the damage function for the K&C model, it is essential to understand the softening stage of UHPC. When UHPC is subjected to tensile stress, it behaves elastically until a portion of its tensile strength, at which microcracks start to develop, called the hardening stage. After reaching tensile capacity, UHPC enters the softening stage where cracks localize in a single crack, and the fracture energy G_f accelerates the propagation of this crack up until failure. On the other hand, UHPC, under compressive stress, unlike its state under tensile stress, has various failure modes such as shear and crushing.

Under uniaxial compression, UHPC behaves elastically until its compressive strength. After that, it enters the softening stage, which is influenced by the presence of fiber reinforcement.

The K&C model implements the damage function to control the rate of hardening and softening stages. Since UHPC is more sensitive to fracture energy, the damage parameters b1, b2, and b3 should be fixed while calibrating the damage function Yasser (2022). The damage function must be adjusted according to UHPC's desired hardening and softening behavior.

After conducting iterations, the 13 pairs of the damage function can be found in Table 3.3. Furthermore, the omega value describes the volume expansion and it affects the model response when confinement is applied. The omega value is recommended to be 0.75 when confinement is absent and 0.9 when confinement is present (Crawford et al. 2014).

Table 3.3 The calibrated K&C damage parameters.

b1	b2	b3	λ	η
1	0.5	1.15	0	0
			8.00e-6	0.80
			6.00e-5	0.93
			9.00e-5	0.99
			1.50e-4	1.00
			3.00e-4	0.98
			8.00e-4	0.87
			1.70e-3	0.63
			2.80e-3	0.40
			4.60e-3	0.25

3.4 Numerical analysis result

The calibrated K&C model is validated using a uniaxially compressed partially fixed single element. The selected element size is 50 mm by 50 mm by 50 mm, and the displacement is applied at a rate of 0.5 mm/sec on the four top nodes (N5 to N8). The single-element setup is shown in Figure 3.6. The single-element analysis result agrees with Zhang's empirical model in Figure 3.7, proving that the calibration of the K&C material model is successful.

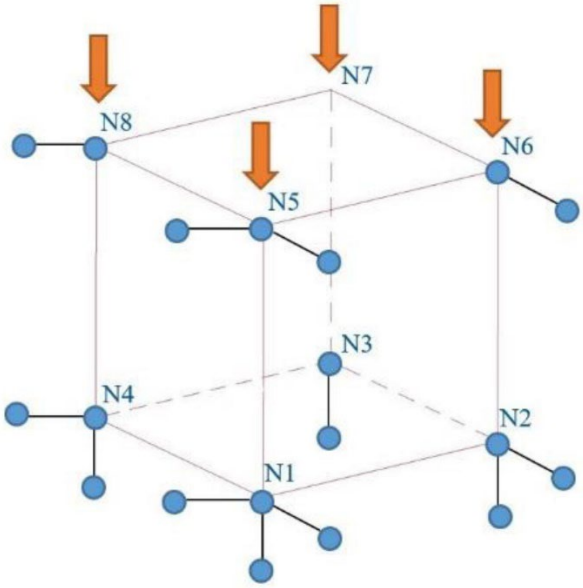

Figure 3.6 Single element model setup under uniaxial compression.

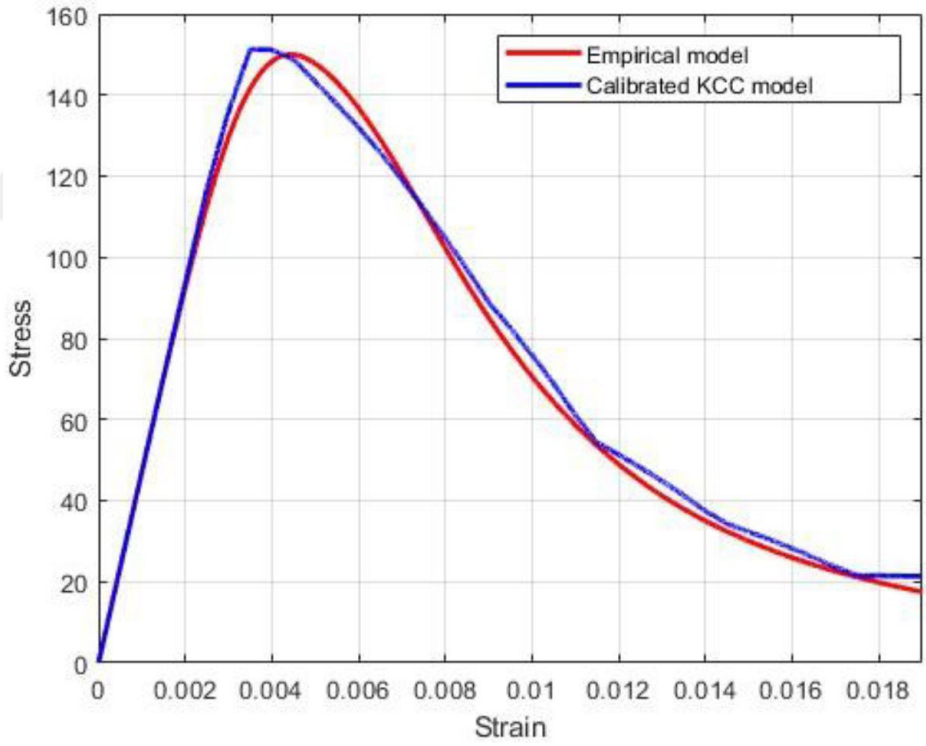

Figure 3.7 Comparison between stress-strain curves of Zhang's empirical model and single element analysis with the calibrated K&C material model.

CHAPTER FOUR
CALIBRATION OF MOHARRAMI AND KOUTROMANOS MATERIAL MODEL

4.1 Introduction

The material model proposed by Moharrami and Koutromanos, (2016) is a multiaxial model capable of analyzing concrete materials under various loading conditions. This elastoplastic model utilizes a nonassociative flow rule for compression behavior and a rotating smeared-crack model for tension behavior and tension-induced cracks.

Moharrami and Koutromanos, (2016) first proposed the triaxial material model to analyze RC structures under cyclic loading conditions. It has been proven to capture various structural elements' material behavior and hysteretic response, such as beams, columns, and beam-to-column joints (Moharrami & Koutromanos, 2016).

El-Helou et al. (2020) further improved the model by including parameters that can analyze fiber-reinforced cementitious materials (FRCM), including UHPC. The improved material model has several excellent features, including the ability to capture the effect of fibers on the crack distribution, confinement, and the effect of fiber orientation on the concrete material response.

This study presents the detailed calibration of the material model proposed by Moharrami and Koutromanos, (2016), followed by implementing the material model and validating the calibrated parameters using test data.

4.2 The triaxial material model overview

One excellent and recently developed FE program is FE-MultiPhys, which can analyze various elements using different materials under static and dynamic events. The program utilizes a combination of algorithms that help depict certain behaviors, such as failure patterns and phase-field solutions.

The triaxial material model proposed by Moharrami and Koutromanos, (2016) is one of the material models available in the FE-MultiPhys program, and the name is CONMRMG. It provides various excellent capabilities to describe the behavior of concrete materials, such as fracture energy, hardening and softening behavior, and fiber effects. The latest version of the triaxial material model aims to capture the behavior of FRCM, which is divided into two components in this material model, with the first one as the contribution of the cementitious matrix σ_c and the second one being the contribution of fibers σ_f as illustrated in Figure 4.1.

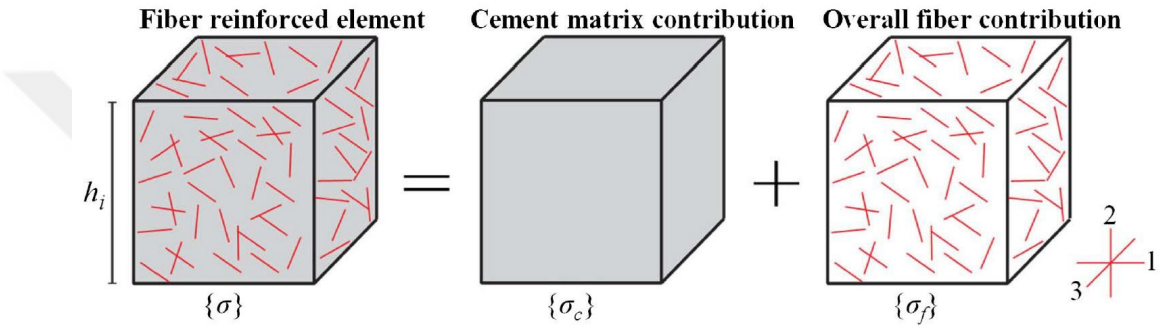

Figure 4.1 Stress vector in RVE for fiber-reinforced cementitious material, expressed as the sum of contributions from cementitious matrix and fibers (El-Helou et al. 2020).

The elastoplastic portion that describes to compression-related stress state of the concrete material consists of a nonassociative flow rule and an isotropic hardening/softening law. The yield surface by Kang et al. (2000), is utilized in the elastoplastic formulation and it is compared to the Drucker–Prager surface in Figure 4.2(a). The following expression describes the formulation:

$$f(\{\hat{}\sigma\},\kappa) = \frac{1}{1-\alpha}\left[\alpha\,.\,I_1 + r(\theta,e)\sqrt{3J_2}\,\right] - c_c(\kappa) = 0 \qquad (4.1)$$

where I1 and J2 = first invariant and second deviatoric invariant of the stress tensor; c_c is the strength parameter which can be considered as the uniaxial compressive strength; κ is the hardening variable describing the accumulation of inelastic deformation; α is a dimensionless parameter expressing the effect of confinement; and $r(\theta, e)$ is the quantity describing the effect of the third deviatoric invariant on the yield

criterion (Kang et al., 2000). The strength of the material changes with the accumulation of inelastic strains by the following hardening softening law Lee and Fenves (1998):

$$c_c(\kappa) = \frac{f_o}{A}\left[(1+A)\sqrt{\varphi(\kappa)} - \varphi(\kappa)\right] \geq f_{res} \tag{4.2}$$

Where $\varphi(\kappa) = 1 + A(2+A)\kappa$; and f_o and A are material constants. Figure 4.2(b). depicts the variation of the strength parameter c_c and κ, and it shows shat the maximum c_c value is f_c at $\kappa = \kappa_o$ where κ_o and A can be obtained if the strain ε_o at peak compressive strength f_c (for the uniaxial stress state) and the area g_c under the hardening-softening plot is known.

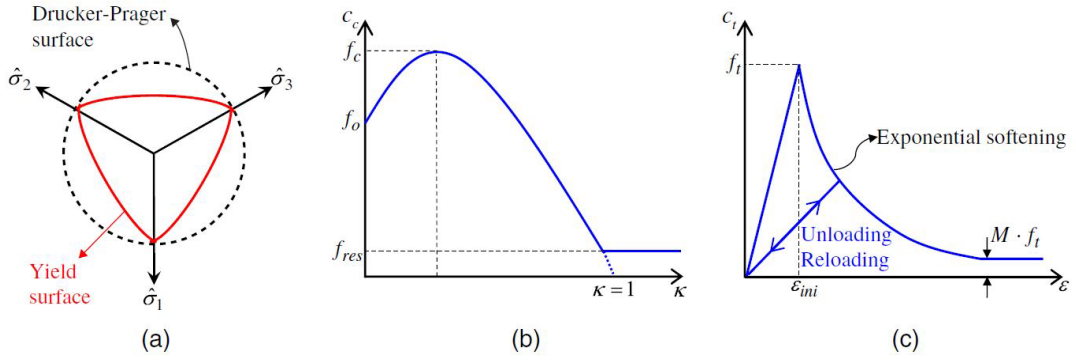

Figure 4.2 Cement matrix constitutive law: (a) yield surface in the deviatoric plane; (b) compression hardening-softening law; and (c) crack model (El-Helou et al. 2020).

To eliminate the effect of localization in the finite element analysis caused by spurious mesh-size, the material parameter g_c must set equal to G_c/h, where G_c is the compressive fracture energy; and h is the element size (Moharrami & Koutromanos, 2016).

The rotating smeared-crack model describes the damage induced by tensile cracking by allowing up to three cracks to occur simultaneously. Cracking is assumed to occur when the principal stress reaches the threshold value c_t. Figure 4.2(c) depicts the softening law and the loading/unloading behavior of the cracked material. The

principal stress σ_i in the crack direction i of the material is expressed by the following equation:

$$\sigma_i = c_t.\left[(1-M)e^{-\lambda_t \frac{\varepsilon_i - \varepsilon_{ini}}{f_t}} + M\right], \qquad i = 1,2,3 \tag{4.3}$$

Where M is the ratio of the residual tensile strength to the tensile strength; ε_{ini} is the strain at onset of cracking; and $\lambda_t$is the parameter controlling the rate of degradation of the post-cracking tensile strength. The parameter c_t is obtained using the following expression:

$$c_t = |x| = \begin{cases} f_t, & \kappa \leq \kappa_o \\ \frac{c_c}{f_c} f_t, & \kappa > \kappa_o \end{cases} \tag{4.4}$$

Where f_t is the uniaxial tensile strength.

4.2 The calibration procedure of the triaxial material model for UHPC

While calibrating the K&C material model is a challenging task due to the complex nature of the material model and UHPC, calibrating the triaxial material model proposed by Moharrami and Koutromanos, (2016) is relatively easier, and it requires tensile and compression test data of UHPC to calibrate the corresponding parameters.

The material model consists of six lines of parameters; each line describes a specific part of the concrete material behavior and consists of 8 input parameters. To calibrate the triaxial material model for UHPC, the three main groups of parameters (compression, tension, and fiber) must be calibrated according to the corresponding test data available in the literature.

The first line has the general parameter for UHPC and does not require any calibration. The first line parameters are presented in Table 4.1.

Table 4.1 The first line of parameters for the triaxial material model.

Parameter	**Value**
E (Elastic modulus) (MPa)	53700
v (Poisson ratio)	0.17
G (Shear modulus) (MPa)	19893.125
K (Bulk modulus) (MPa)	26524.167
Number of sub-increment steps in the stress update algorithm	1
This is a parameter that controls material failure	1
Maximum number of iterations in stress update algorithm	100
Tolerance for convergence in stress update algorithm	1.e-8

This study calibrates the compression parameters by modeling and analyzing a cylinder under uniaxial compression and comparing the result to the test data for validation. The tension parameters will be calibrated according to the Direct Tensile Test (DTT) database provided by Salah and Kalliontzis (2023). Finally, the calibrated triaxial material model will be assessed by utilizing it to analyze a corbel example from the literature, and the results will be compared in Chapter 6.

4.2.1 Calibrating the UHPC Compression Parameters

Calibrating the second line of parameters corresponding to the compressive behavior of UHPC is carried out by obtaining the uniaxial compression test data from Helou (2016) and Xu and Wille (2014). The test specimens Helou (2016) used were cylindrical specimens with a diameter of 76 mm and a height of 165 mm, which were also modeled with the exact dimensions as shown in Figure 4.3. The parameters obtained from the tests are used in the triaxial material model to analyze the cylinder model. The cylinder was modeled using solid elements and is subjected to an axially monotonic load applied as a constant displacement by the top plate while the bottom plate is fixed. The parameters used in the finite element analysis are presented in Table 4.2.

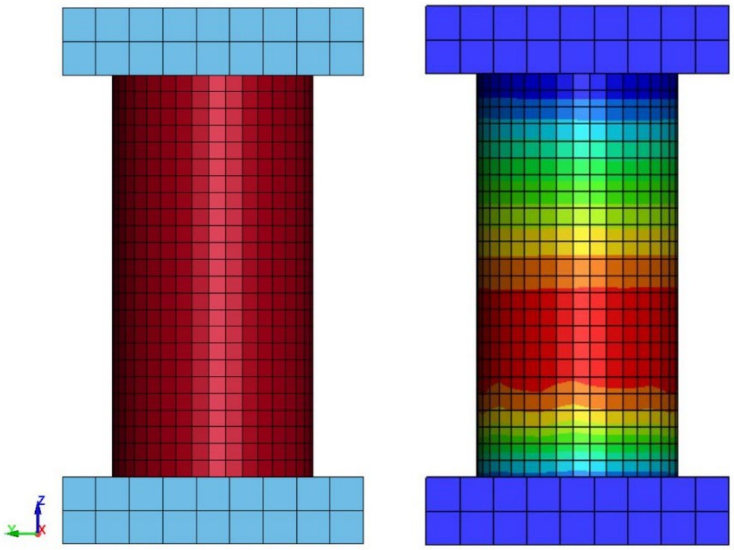

Figure 4.3 Finite element model of the UHPC cylinder specimen under compression.

Table 4.2 The second line of parameters for the triaxial material model.

Parameter	Value
f_c (Uniaxial compressive strength) (MPa)	150.0
ε_0 (strain corresponding to peak compressive stress)	0.0043
f_{cres}/f_c (Residual compressive strength factor)	0.1
f_{c0} (Value of initial yield stress) (MPa)	80.0
G_c (Compressive fracture energy) (KN/m)	70.0
ɑ (Confinement factor)	0.4
α_p (Dilatancy factor)	0.2
d (Ductility factor)	11

The stress-strain result from the analysis in Figure 4.4 shows a good agreement with the test result from Xu & Wille (2014), which means that the compression parameters of the triaxial material model have been successfully calibrated.

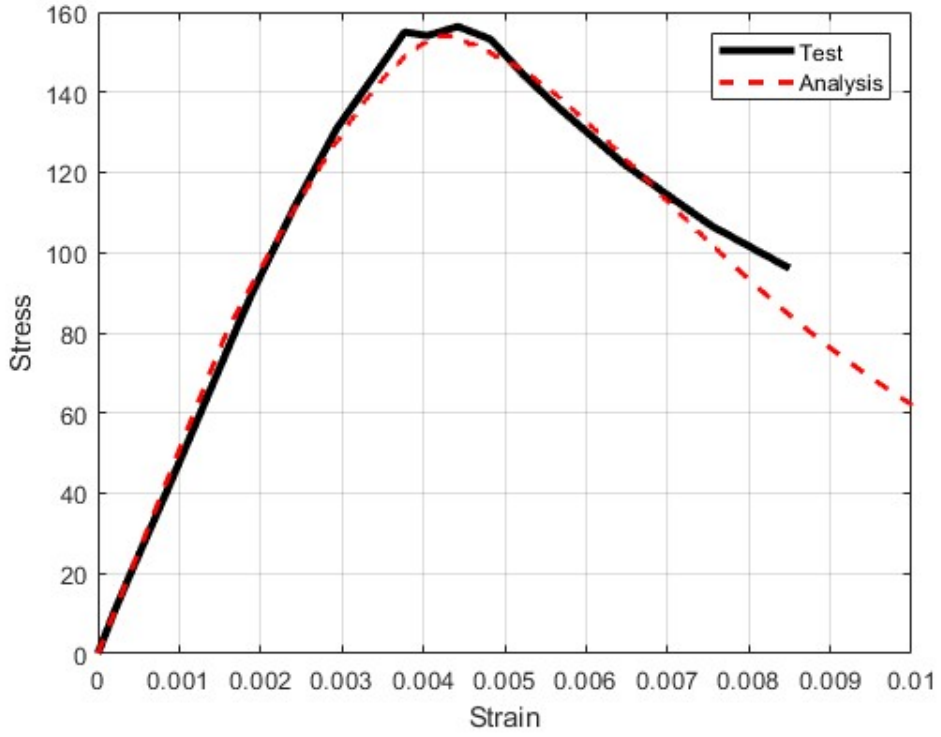

Figure 4.4 Comparison between the stress-strain result of the triaxial material model and test result from Xu & Wille (2014) in terms of uniaxial compression.

4.2.2 Calibrating the UHPC Tension Parameters

While some triaxial material model tension parameters can be directly calibrated by obtaining test data, other parameters can be calibrated using existing formulas in the literature. The tensile strength f_t parameter is taken directly from DTT provided by Salah and Kalliontzis (2023). On the other hand, the post-cracking slope parameter λ_t/f_t, the residual tensile strength factor f_{tres}/f_t, and the fracture energy related to tensile softening G_f can be obtained using empirical methods. However, there is no need to calibrate the tensile fracture energy if the post-cracking slope parameter and the residual tensile strength factor are calibrated and vice versa. In this study, the calibration of the post-cracking slope parameter and the residual tensile strength factor are chosen to be calibrated.

To calibrate the post-cracking slope parameter, the parameter controlling strength degradation λ_t must be obtained first, which is calculated using the following equation by Helou (2016):

$$\lambda_t = \frac{(1-M){f_t}^2}{G_t} h \tag{4.5}$$

Where M is the ratio of the residual tensile strength over the tensile strength f_{tres}/f_t; G_t is the tensile fracture energy. The complete set of the UHPC tension parameters is shown in Table 4.3.

Table 4.3 The third line of parameters for the triaxial material model.

Parameter	Value
f_t (Tensile strength) (MPa)	6.5
λ_t/f_t (Post-cracking slope parameter)	4582.5
f_{tres}/f_t (Residual tensile strength factor)	0.01
G_t (Tensile fracture energy) (N/m)	60.0
P5	Not in use
P6	Not in use
P7	Not in use
P8	Not in use

4.2.3 Calibrating the UHPC Steel Fiber Parameters

4.2.3.1 Fibers orientation

The effect of fiber in the cementitious matrix is governed heavily by the fiber orientation within the matrix, which means that every fiber must be considered during analysis. However, this would lead to a very costly computational effort. The proposed triaxial material model allows the assumption of fibers to be aligned in one of the three Cartesian coordinate spaces, $i = 1, 2, 3$. Fibers are assumed to provide resistance along their axial direction contributing to the material's normal stress component Helou (2016). The total normal stress along the Cartesian direction i is expressed as the following:

$$\sigma_{ii} = \sigma_{cii} + \rho_{f_i} v_f \sigma_{f_i} \tag{4.6}$$

Where σ_{cii} is the cementitious matrix stress; v_f is the fiber volume; σ_{f_i} is the fibers axial stress in the direction i; ρ_{f_i} is the weighting factor representing the volumetric fraction of fibers oriented in a specific direction. The sum of the three weighting factors in all directions must equal 1 as follows:

$$\rho_{f_1} + \rho_{f_2} + \rho_{f_3} = 1 \tag{4.7}$$

Assigning the value of the fiber's volumetric fraction in its corresponding direction depends on the desired fiber distribution. The value of ρ_{f_i} varies from 0 when no fibers are oriented in a certain direction i, to 1 when all fibers are oriented in that direction. In the case of randomly distributed fibers, the value 1/3 is assigned for all the weighting factors.

The typical scenario in concrete pouring is that most of the fibers align in the flow direction, while the perpendicular directions receive fewer fibers. The assumption in El-Helou et al. (2020) is that if the factor corresponding to the flow direction is μ_1, the other two factors are equal $\mu_2 = \mu_3$. Helou (2016) proposed a relation between μ_1 and $\mu_2 = \mu_3$, which is presented in Figure 4.5. Equation (29) was obtained from the relation proposed by Helou, (2016).

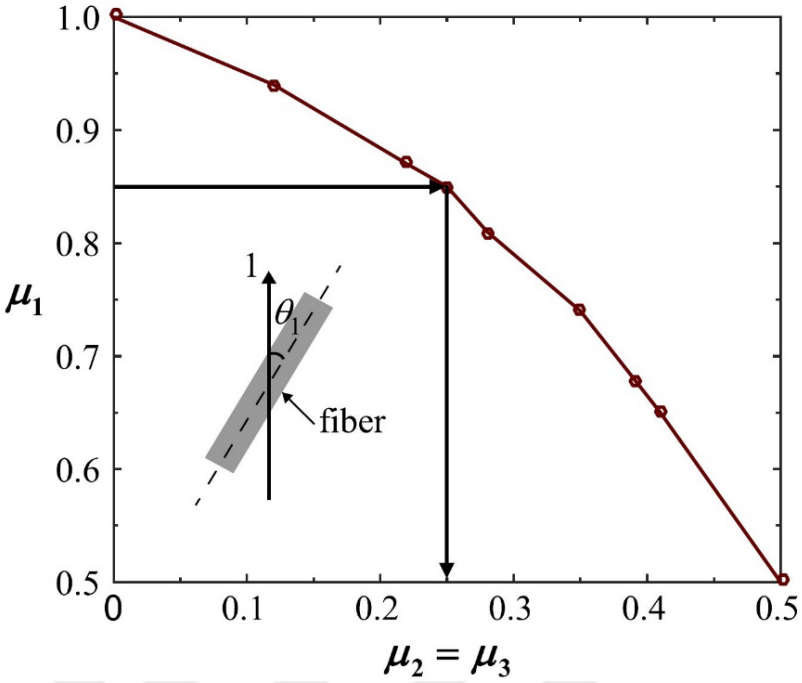

Figure 4.5 The relation between μ_1 and $\mu_2 = \mu_3$ (El-Helou et al., 2020).

$$\mu_1 = 1.001 - 0.2156X_{\mu_2=\mu_3} - 1.6X_{\mu_2=\mu_3}{}^2 \tag{4.8}$$

Where $X_{\mu_2=\mu_3}$ is the parameter representing the value of $\mu_2 = \mu_3$.

4.2.3.1 Distributed cracking due to fiber presence

When the cementitious matrix cracks, fibers help bridge this crack by developing an axial force that prevents the crack from opening further. In a typical scenario, the formation of the first crack is followed by the localization of strains in a single crack, resulting in an accelerating degradation of strength in the post-cracking portion of the stress-strain curve. On the other hand, when the cementitious matrix is reinforced with fibers, the crack-bridging effect helps increase the tensile strength of the post-cracking portion of the stress-strain curve, which increases the ductility of concrete (El-Helou et al., 2020).

El-Helou et al. (2020) proposed a relation presented in Figure 4.6 to account for the formation of multiple cracks in the cementitious matrix due to the crack-bridging effect of fibers.

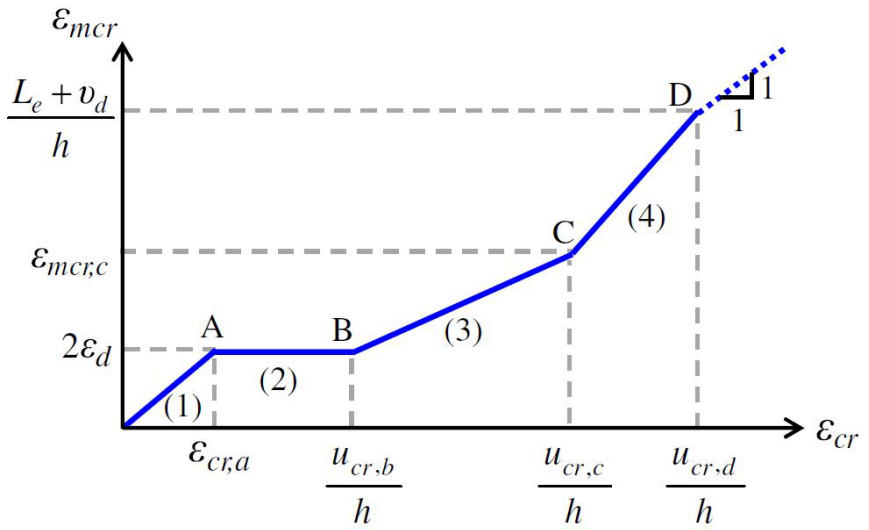

Figure 4.6 Modified cracking strain and crack opening to account for multiple cracks in fiber-reinforced cementitious materials (El-Helou et al., 2020).

The curve is established by calibrating five parameters $\varepsilon_{cr,a}$, $u_{cr,b}$, $u_{cr,c}$, , $u_{mcr,c}$, and , $u_{cr,d}$. These five parameters established the four points on the curve: A, B, C, and D, connecting five segments in the curve, with each segment representing a different stage in the material's behavior. Segment (1), which starts from the origin and ends at point A, represents the stage where the crack displacement reaches the threshold value v_d described by the following equation:

$$v_d = \frac{2\tau_0 {L_e}^2}{E_f d_f} \tag{4.10}$$

Where τ_0 is the frictional stress of fiber-matrix; L_e is the embedment length of fibers; E_f is the modulus of elasticity of fibers; d_f is the diameter of fibers. Segment (2) starts from point A until point B where the cracking strain reaches the value $u_{cr,b}/h$. Segment (3) and (4) are reached the further tensile deformations cause the localization

of strains in a single crack. This localization begins slowly in segment (3) until the cracking strain reaches the value $u_{cr,c}/h$. Segment (4) has a slope more than 1, which means that the strain increases with a fast rate until the craking strain reaches the value $u_{cr,d}/h$ (El-Helou et al. 2020). The calibration of the strain adjustment function's parameters is carried out by matching the result of a single element analysis to experimental data shown in Figure 4.7. The first input is defined as:

$$\varepsilon_{cr,a} = \varepsilon_a - \varepsilon_{ini} \tag{4.11}$$

Where ε_a is the cracking strain at the first crack; $\varepsilon_{ini} = f_t/E$, which is the unreinforced matrix cracking strain. The rest of the parameters are given in terms of total displacement to make sure that the material model is mesh-objective and are calculated as follows:

$$d_b = (\varepsilon_b - \varepsilon_{ini})h_y \tag{4.12}$$

$$d_c = (\varepsilon_c - \varepsilon_{ini})h_y \tag{4.13}$$

Where ε_b and ε_c are the strain at the start of the softening behavior and strain at the localization of fine cracks strains in one single crack respectively; h_y is the element length. The post-peak parameter d_e is obtained directly from the stress-strain curve in Figure 4.7. The last paremeter d_d marks the total tensile capacity loss in the material where fibers are completely pulled out Helou (2016). The full set of the calibrated tensile and fiber parameters are presented in Table 4.4 and Table 4.5.

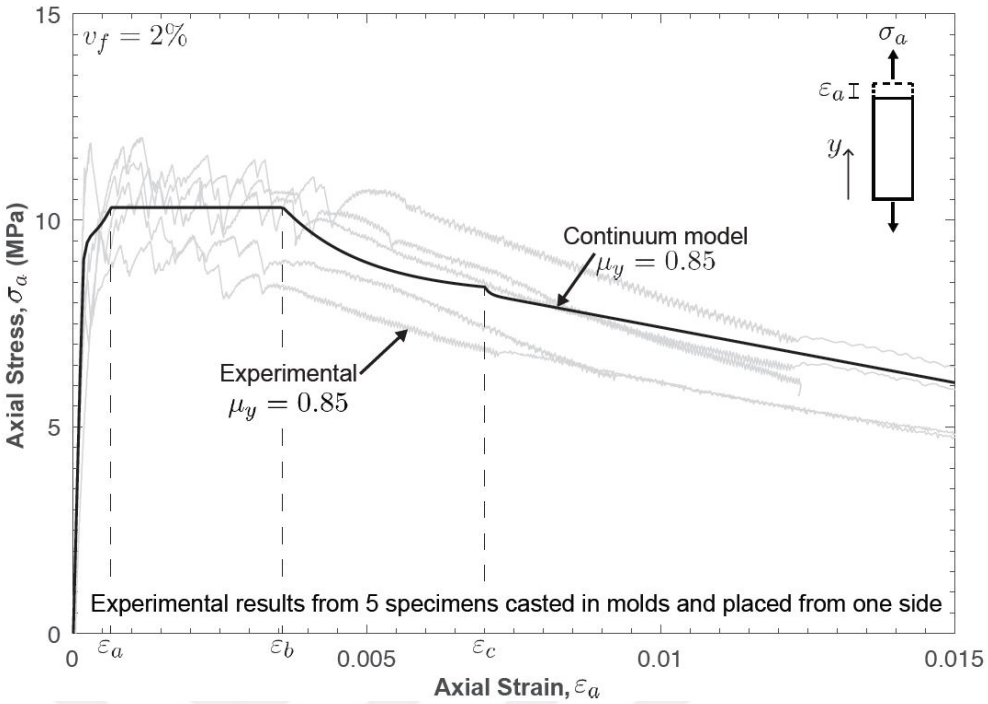

Figure 4.7 Simulated uniaxial tensile stress-strain response for UHPC for identifying the strain adjustment function parameters (El-Helou, 2016).

Table 4.4 The fifth line of parameters corresponding to fiber characteristics.

Parameter	**Value**
E_f (Elastic modulus of fibers)	205000
L_e (Shortest embedment fiber length)	2.5
d_f (fiber diameter) (mm)	0.2
G_{df} (Cohesive strength parameter)	0.0
τ_0 (Frictional stress of fiber-matrix) (MPa)	10
β (Parameter affecting the bond-slip response of the fiber)	0
σ_0 (bond-slip law parameter)	0
ρ_f (Fiber volumetric content) (%)	2

Table 4.5 The sixth line of parameters corresponding to fibers modified strain parameters and orientation.

Parameter	Value
$\varepsilon_{cr,a}$	0.00043
d_b (mm)	0.28
d_c (mm)	0.86
d_d (mm)	2.967
d_{me} (mm)	0.04
μ_1	0.42
μ_2	0.63
μ_3	0.42

The DTT specimen from Salah and Kalliontzis (2023), which is shown in Figure 4.(a) is modeled and analyzed using the calibrated parameters to assess its' accuracy. The finite element model of the DTT specimen is presented in Figure 4.8(b)

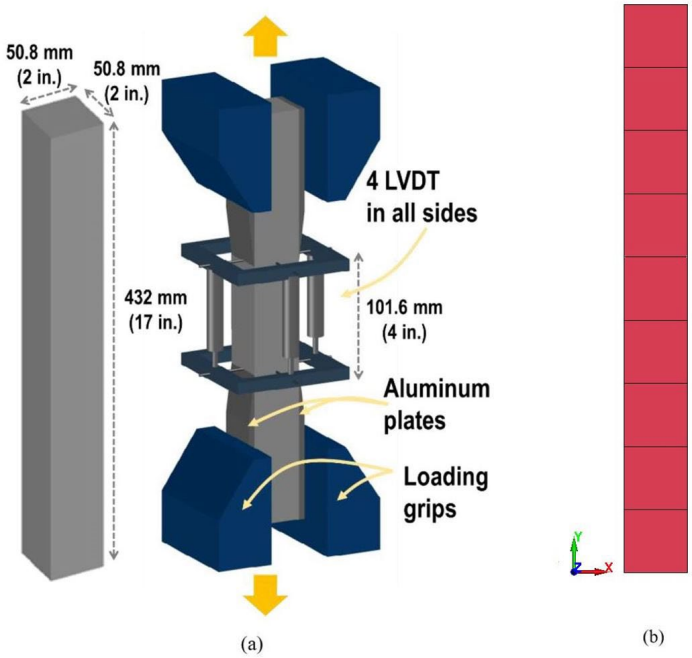

Figure 4.8 (a) DTT specimen details and test setup by Salah and Kalliontzis (2023); (b) DTT finite element model.

The specimen was modeled in the LS-PrePost program using hexahedral elements, and the tension is applied in the axial direction in a displacement-controlled manner. The analysis was carried out using the FE-MultiPhys program. The analysis result compared to the test data obtained by Salah and Kalliontzis (2023) in Figure 4.9 shows a strong agreement, which means that the calibration procedure provided reliable parameters that can be used in more complex models.

The triaxial material model is used to analyze corbels made of UHPC to further investigate the model's reliability in predicting the actual behavior of UHPC. The modeling process and analysis result is discussed in Chapter 6.

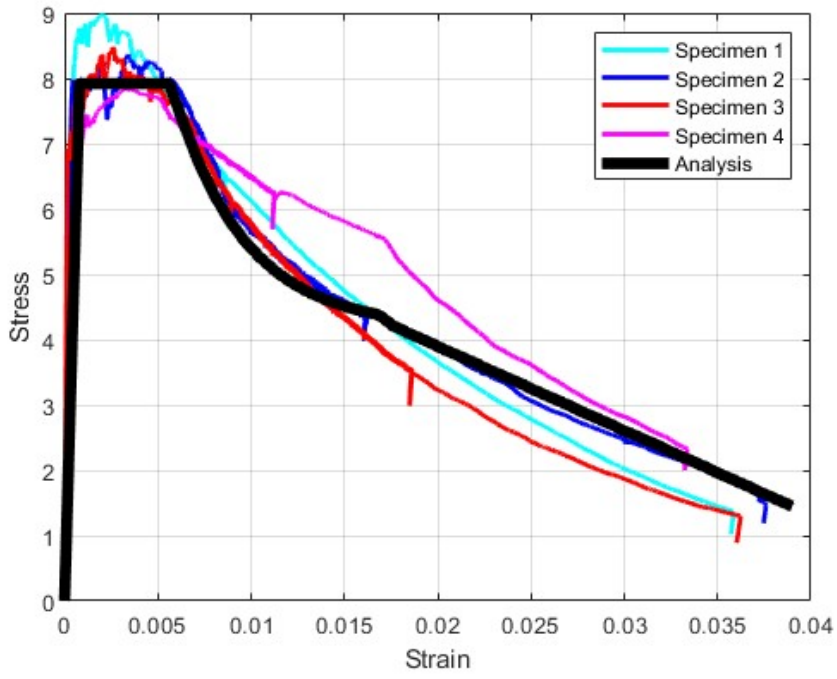

Figure 4.9 Comparison between analysis result and test data collected from Salah and Kalliontzis (2023) regarding tensile stress-strain.

CHAPTER FIVE
FINITE ELEMENT ANALYSIS RESULTS

5.1 Introduction

To further assess the reliability of the calibrated K&C, triaxial material model by Moharrami and Koutromanos (2016), and the modified strut-and-tie model, a corbel specimen from Ridha et al. (2017) has been chosen to be modeled and analyzed using the three previously mentioned methods and the results are compared.

This chapter discusses the specimen properties, finite element modeling procedure, and analysis results in detail.

5.2 Corbel specimen properties

Ridha et al. (2017) conducted an experiment on eleven UHPC corbel specimens to investigate the effect of shear-span to depth ratio, main tension reinforcement ratio, and secondary reinforcement ratio on the behavior of UHPC corbels. The test results show the effectiveness of using UHPC, which is reflected in the force-displacement curves, stiffness, ductility, and cracking pattern.

In this study, one particular specimen (C4G2) is picked to be modeled and analyzed. The test setup shown in Figure 5.1 depicts the loading scheme, arrangement of reinforcement, and corbel's dimensions.

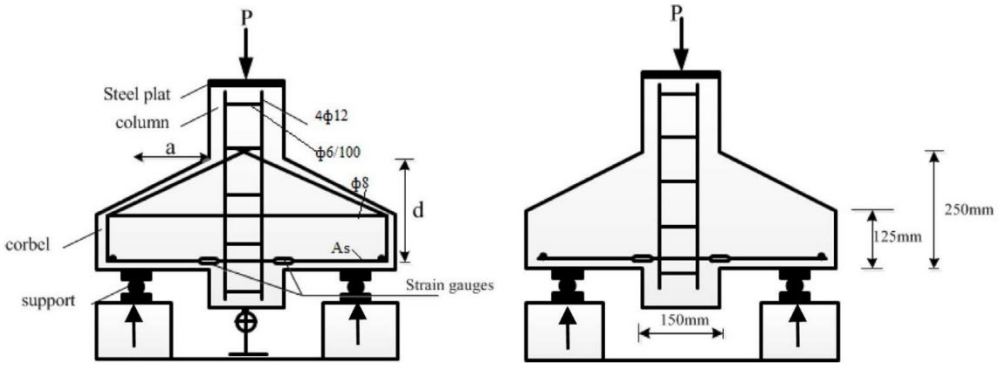

Figure 5.1 Steel arrangement and geometry and loading scheme of the corbel specimen (Ridha et al. 2017).

The column dimensions are 150 mm by 150 mm with a height of 450 mm. The column supports two corbel cantilevers from two sides with a projection length of 250 mm, a corbel height of 250 mm at the face of the column, and 125 mm at the free end, and the shear-span to depth ratio is 0.4. The corbel is subjected to three-point flexural loading as seen in Figure 5.1.

The main tension reinforcement in the UHPC corbel specimen consists of two bars with a diameter of 12 mm. In contrast, secondary reinforcement bars are 2 closed stirrups with a diameter of 8 mm placed with a 70 mm spacing starting from the center of the main tension reinforcement. The shear reinforcement consists of 6 mm stirrups with a spacing 100 on the center of the corbel's column. The concrete cover is taken as 40 mm. The UHPC characteristics used in this test, alongside main and secondary reinforcement steel properties, are presented in Table 5.1.

Table 5.1 Materials properties.

Material	**Property**	**Average**
UHPC	Compressive strength (MPa)	150
	Peak strain (%)	0.45
	Tensile strength (MPa)	15
	Flexure tensile strength (MPa)	18.3
Rebar	Yield strength of 12 mm bars (MPa)	419
	Yield strength of 8 mm bars (MPa)	302
	Ultimate strength of 12 mm bars (MPa)	590
	Ultimate strength of 8 mm bars (MPa)	422
	Modulus of elasticity (GPa)	200
Steel fibers	Type	Straight
	Tensile strength (MPa)	2600
	Density (kg/m^3)	7800
	Aspect ratio, L_f/D_f	13/0.2=65

5.3 Finite element modelling procedure for the K&C material model

The corbel is modeled as a half model for simplicity using the LS-PrePost program, which is available as a free license for students. The corbel's concrete part, shown in Figure 5.2 (b), is modeled using hexahedral elements (solid elements), consisting of 978 solid elements and 1521 nodes. The corbel has been modeled as a half model utilizing the symmetrical nature of the specimen for simplicity. The left side of the half model has been restrained in the horizontal direction while the corbel left end is free to move. The solid elements are single point integrated with ELFORM = 1, and the UHPC was applied using the K&C (MAT_CONCRETE_DAMAGE_REL3) material model with the calibrated parameters obtained in Chapter 3. According to LS-DYNA Manual R13.0 Vol I, Hourglass control type 6 must be used with 3D elements. The Hourglass coefficient has been calibrated in this study to match the test data. It is taken as 0.001 for concrete solid elements, and the default value (0.1) is taken for elastic solid elements.

The bottom plate placed at the location of the applied load is modeled as solid elements with the elastic material model (MAT_ELASTIC). The reason why it is modeled using elastic elements is to avoid any localized failure at the points where concentrated load is applied. The procedure presented by Canha et al. (2014) to model the supports is adopted in this study. The two supports at the shear-span distance on each corbel consist of two parts with a contact surface (CONTACT_AUTOMATIC_SURFACE_TO_SURFACE) inclined at a 45^{o} angle to resample the test setup. The parameters used for the elastic material model are presented in Table 5.2.

Table 5.2 Elastic material model parameters.

Parameter	Value
Mass density (g/mm^3)	2.400e-09
Young's modulus (GPa)	200.0
Poisson's ratio	0.2

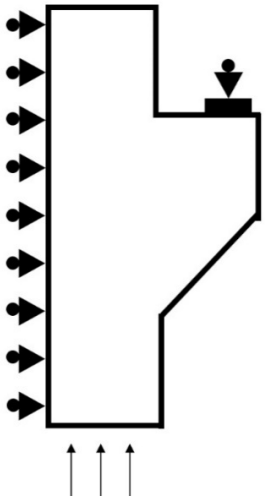

(a)

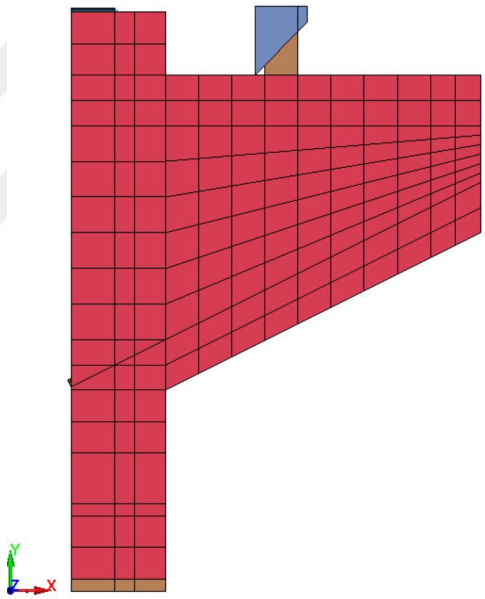

(b)

Figure 5.2 (a) Schematic drawing of the model, (b) finite element model of the C4G2 UHPC corbel specimen.

The reinforcement bars are modeled using beam elements with a total number of 144 elements as shown in Figure 5.3. Due to the inconsistency of the mesh size and shape, main tension reinforcement bars have shared nodes with the solid elements of the corbel and the column, while secondary reinforcement is constrained inside the solid elements using the keyword (CONSTRAINED_LAGRANGE_IN_SOLID). The

material model named (MAT_PLASTIC_kINEMATIC) is used to model the reinforcement bars with the parameters presented in Table 5.3.

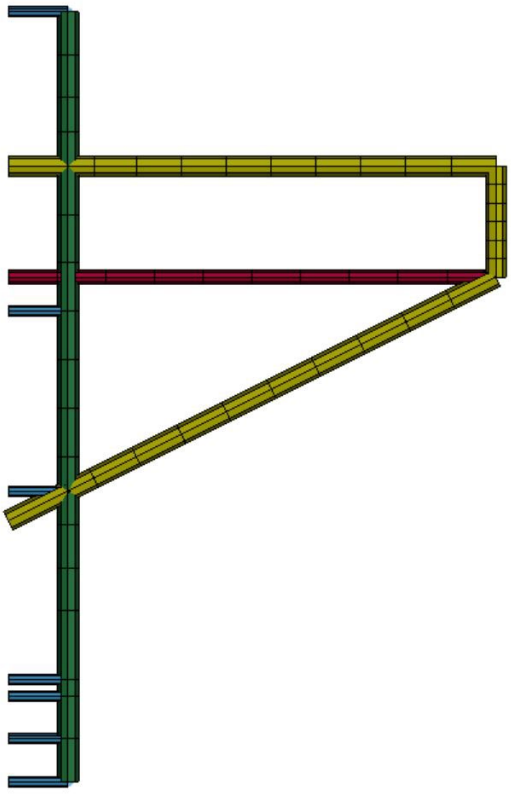

Figure 5.3 Reinforcement bars modeled in LS-PrePost.

Table 5.3 Plastic kinematic material model parameters.

Parameter	Value
Mass density (g/mm^3)	7.850e-09
Young's modulus (GPa)	200.0
Poisson's ratio	0.3
Yield stress (MPa) for 12 mm bars	419.0
Yield stress (MPa) for 8 mm bars	302.0

The monotonic load distributed on a number of 28 nodes defined as set in (SET_NODE_LIST) at the bottom of the elastic plate as shown in Figure 5.4 is applied in a displacement-controlled manner with a rate of 1 mm/sec using the card (BOUNDARY_PRESCRIBED_MOTION_SET) and the displacement rate is assigned in the keyword card (DEFINE-CURVE). The analysis was run in an explicit manner.

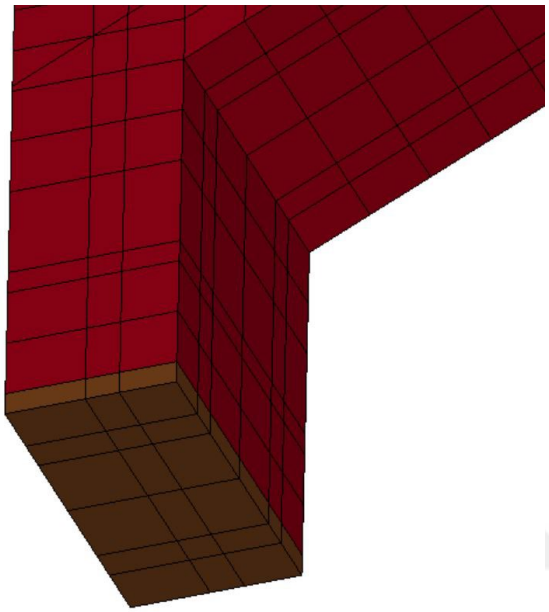

Figure 5.4 The location of the applied displacement in the finite element model of the corbel specimen.

5.3.1 Finite element result for the UHPC corbel modeled using the K&C material model

The finite element analysis result for the UHPC corbel presented in Figure 5.5 shows a strong agreement with the test result of the C4G2 specimen from Ridha et al. (2017). The finite element results in output an ultimate shear capacity of 1660 KN for the UHPC corbel, while the test result shows that the actual ultimate load of the UHPC corbel is 1658.5 KN. This result proves that the calibration procedure of the K&C material model is successful, and it is reliable to be used for the modeling of any UHPC structural element given that the UHPC test data is known.

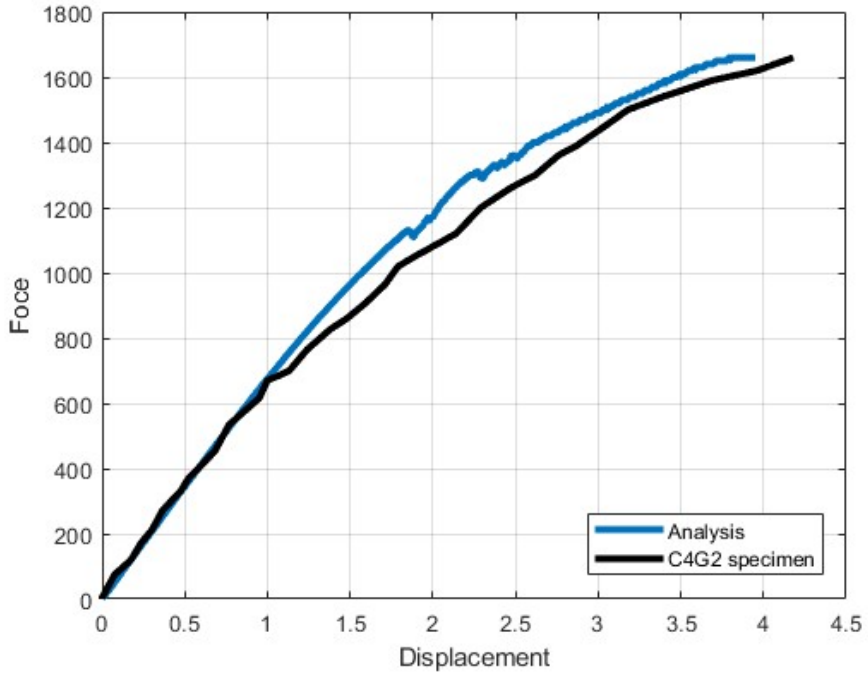

Figure 5.5 Comparison between finite element results and the test data for the UHPC corbel specimen (C4G2) from Ridha et al. (2017) in terms of force-displacement.

5.3 Finite element modeling procedure for the triaxial material model

Modeling the UHPC corbel to be analyzed using the triaxial material model proposed by Moharrami and Koutromanos, (2016) is carried out using LS-PrePost. However, the analysis was carried out using the FE-MultiPhys program. The UHPC corbel's concrete part shown in Figure 5.7 was modeled using solid elements with Hourglass control type (STIFFNESS) with Young's modulus of 53700.0 MPa and Hourglass coefficient of 0.01. The UHPC is applied using the triaxial material model named (CONMRMG) with the calibrated parameters obtained in Chapter 4.

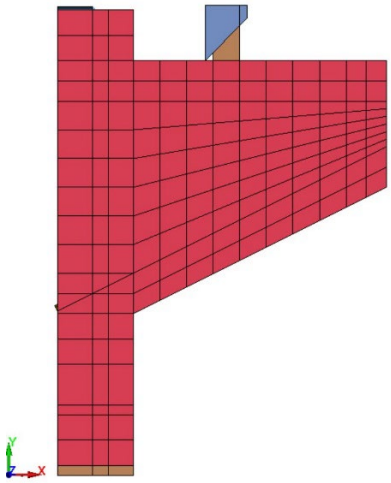

Figure 5.6 Finite element model of the C4G2 UHPC corbel specimen to be analyzed using FE-MultiPhys program.

The main and secondary reinforcement bars are modeled using beam elements, as seen in Figure 5.3. The material model used to apply steel material for the reinforcement bars is (STEEL01) with the parameters presented in Table 5.4.

Table **5**.4 STEEL01 material model parameters.

Parameter	**Value**
Young's modulus (GPa)	200.0
Initial yield stress (MPa) for 12 mm bars	419.0
Initial yield stress (MPa) for 8 mm bars	302.0

The plate at the bottom alongside the two supports located at the shear-span distance of each corbel is modeled using solid elements and the elastic material model was applied using steel parameters. However, the two supports on top of each corbel consist of two parts with an inclined interface between these two parts as seen in Figure 6.8. The interface between the two parts is modeled using interface elements with a thickness of 50 mm, and the material model named (INTERF3D) is used to apply the contact surface between the two separate parts. The parameters used in the (INTERF3D) are calibrated to match the test result, and it is presented in Table 5.5.

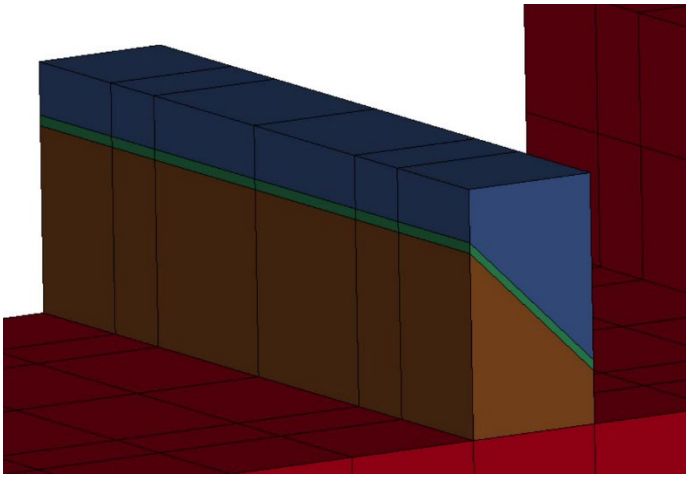

Figure 5.7 The support on the corbel consists of two parts connected using interface elements.

Table 5.5 INTERF3D material model parameters.

Parameter	Value
Normal stiffness (N/mm)	47.0
Shear stiffness (N/mm)	37.0
The rest of the parameters have insignificant effect on the result	

As mentioned in section 5.3, the load is applied in a displacement-controlled manner, and the analysis was carried out implicitly.

5.3 Finite element result for the UHPC corbel modeled using the triaxial material model

The force-displacement result obtained from the finite element analysis in Figure 5.9 is compared to the one obtained from the test conducted by Ridha et al. (2017). The result shows a strong agreement with test data, proving that the triaxial material model is more accurate than the K&C material model. The triaxial material model is also more accurate than the K&C material model in predicting the shear capacity of the UHPC corbel, and the predicted value is 1640 KN.

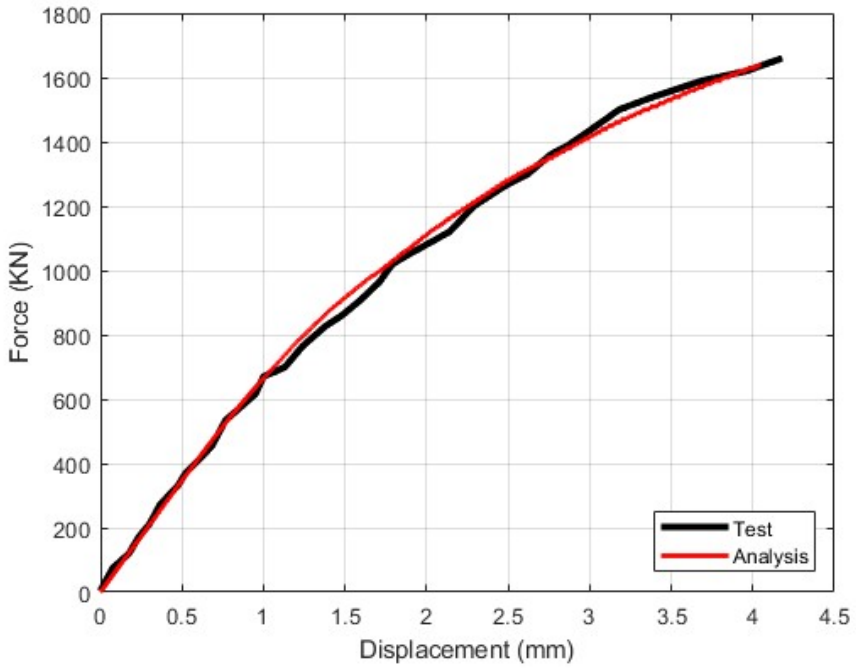

Figure 5.8 Comparison between the finite element result of the UHPC corbel analyzed using the triaxial material model and the test data in terms of force-displacement.

CHAPTER SIX
MODIFIED STRUT-AND-TIE MODEL

6.1 Introduction

The strut-and-tie model has been one of the reliable methods utilized by engineers in the practical field to design D-region structural elements. However, the traditional strut-and-tie model available in design standard codes is developed to design d-region sections made of NSC. It is not suitable to design sections made of UHPC. The behavior of UHPC is different from NSC in terms of ductility, compression, and tensile strength, which means that the traditional strut-and-tie model will not predict the actual behavior of the UHPC elements with acceptable accuracy. In this case, a modified strut-and-tie model must be utilized.

This chapter discusses in detail a modified strut-and-tie model proposed by Huang et al. (2024).

6.2 The modified strut-and-tie model overview

One factor that significantly affects the behavior of UHPC is fibers. In the modified strut-and-tie model proposed by Huang et al. (2024), the contribution of fibers to concrete tensile capacity alongside main and secondary reinforcement is represented as horizontal ties in the top part of corbels. These ties, alongside the concrete strut at the bottom part of corbels, form a truss system, as seen in Figure 6.1.

The modified strut-and-tie model assumes that the failure of any part of the truss system marks the ultimate load-carrying capacity V_u of the corbel, which is expressed as follows:

$$V_u = \min(V_{u,tie}, V_{u,strut}) \tag{6.1}$$

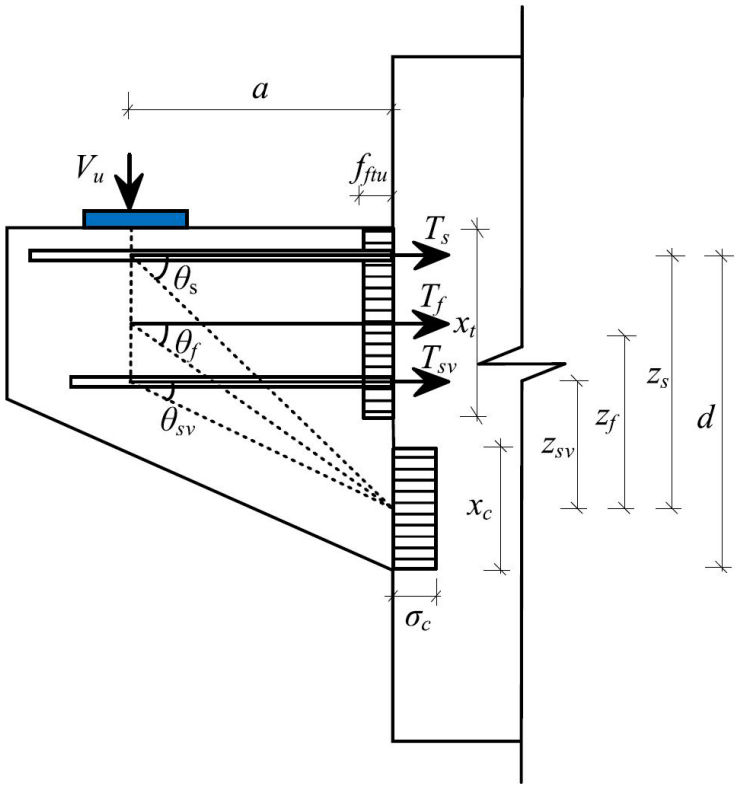

Figure 6.1 Improved strut-and-tie model diagram (Huang et al. 2024).

Where $V_{u,tie}$ and $V_{u,strut}$ are the ultimate vertical loads on corbels when ties and struts reach their ultimate strengths respectively. The tie-controlled vertical force is calculated using the following equation:

$$V_{u,tie} = V_s + V_{sv} + V_f \tag{6.2}$$

Where V_s , V_{sv} , and V_f are the vertical load capacity provided by the main reinforcement, secondary reinforcement, and concrete tension zone tie, respectively. The load capacity contributed by the main reinforcement tie is calculated as follows:

$$V_s = T_s \tan\theta_s = \beta f_y A_s z_s / a \tag{6.3}$$

Where T_s is the tensile force provided by the main reinforcement tie; θ_s is the angle between the main reinforcement tie and concrete strut; f_y is the main reinforcement yield strength; A_s the main reinforcement steel area; z_s is the height of the triangular truss system formed by the internal force provided by main reinforcement; a is the shear span of the corbel; β is the main reinforcement tie adjustment coefficient, and it is obtained from the following expression:

$$\beta = \begin{cases} \frac{f_u}{f_y}, & \rho_u > 0.33\% \\ 1.0, & \rho_u \leq 0.33\% \end{cases} \tag{6.4}$$

Where f_u is the ultimate tensile strength of the main reinforcement and ρ_u is the main reinforcement ratio. According to Huang et al. (2024), the main reinforcement yields and fails faster when the ratio ρ_u falls below 0.33%, which causes the corbel to fail. On the other hand, when the main reinforcement ratio ρ_u is larger than 0.33%, the main reinforcement can contribute to shear resistance even after yielding. Therefore, the adjustment coefficient β must be used to account for the main reinforcement ratio effect on the ultimate capacity of corbels.

The contribution of the secondary reinforcement to the vertical ultimate load of the corbel is calculated using the following equation:

$$V_{sv} = T_{sv} \tan \theta_{sv} = f_{yv} A_{sv} Z_{sv} / a \tag{6.5}$$

Where T_{sv} is the tensile force provided by the secondary reinforcement; θ_{sv} is the angle between the secondary reinforcement tie and concrete strut; f_{yv} represents the yield strength of the secondary reinforcement tie; A_{sv} is the effective area steel of the secondary reinforcement; z_{sv} is the height of the triangular truss system formed by the internal force provided by secondary reinforcement.

It has been revealed that the tensile stress distribution of UHPC corbels at the point of ultimate load can be represented as an equivalent rectangular stress block. The height x_t of that rectangular stress block is calculated as follows:

$$x_t = h - 1.25x_c \tag{6.7}$$

Where h is the height of the corbel; x_c is the height of the compressed zone at the bottom part of the corbel.

The width of the equivalent rectangular stress block f_{ftu} represents the tensile strength of UHPC at the ultimate load and is calculated as follows:

$$f_{ftu} = f_t \beta_{tu} \lambda_f \tag{6.8}$$

Where f_t is the tensile strength of UHPC; β_{tu} represents the influence factor of fibers on the strength of the tensile zone, which is equal to 1.3 in the case of flexural members; λ_f is the fiber volume.

The contribution of UHPC to the vertical ultimate load of the corbel is calculated using the following equation:

$$V_{f1} = T_f \tan\theta_f = f_{ftu} b(h - 1.25x_c) Z_f / a \tag{6.9}$$

Where T_f is the tensile force provided by the UHPC rod; θ_f is the angle between the UHPC rod and the corresponding concrete strut; b is the width of the corbel; Z_f is the height of the triangular truss system formed by the internal force provided by UHPC rod.

The ultimate load of UHPC compression strut which corresponds to the main reinforcement $V_{u,strut}$ is calculated using the following equation:

$$V_{u,strut} = \varphi' \xi_1 f'_c b B_{strut} \sin\theta_s \tag{6.10}$$

Where ξ_1 is an enhancement factor accounting for the effect of steel fibers on the transverse strain in the compression strut of UHPC, and is taken as 1.2; f'_c is the compressive strength of UHPC; B_{strut} is the width of the compression strut, which is taken as $B_{strut} = 0.8x_c$; φ' is the coefficient of shear span-depth ratio influence on

UHPC corbels' compressive strength. The value of φ' is obtained using the following expression:

$$\varphi' = \begin{cases} 1.3, & a/d \leq 0.4 \\ 1.0, & 0.4 < a/d < 0.8 \\ 0.9, & a/d \geq 0.8 \end{cases} \tag{6.12}$$

The height of the compressed zone x_c is obtained by solving the equilibrium of section forces. The equilibrium equation is presented as follows:

$$\sigma_c b x_c = \rho_s b d f_s + f_{ftu} b (d - 1.25 x_c) + f_{yv} A_{sv} \tag{6.13}$$

Where σ_c is the maximum compressive stress at the compressed zone's edge, which is equal to $\xi_0 f'_c$, where ξ_0 is the coefficient of the equivalent rectangular stress block, and it is taken as 1.0.

To calculate the value of z_s, z_{sv}, and z_f, the the value of z_{sv} is assumed to be half of z_s. As a result, the following formulas are derived:

$$z_{sv} = \frac{z_s}{2} = 0.5 \left(d - \frac{x_c}{2}\right) \tag{6.14}$$

$$z_f = h - 0.5 x_c - 0.5 (h - 1.25 x_c) \tag{6.15}$$

6.3 Comparison with finite element results

The modified strut-and-tie model is used in this study to predict the ultimate load of one of the test specimens from Ridha et al. (2017) namely (C4G2). The result is compared to the finite element analysis results obtained from the K&C and the triaxial material model proposed by Moharrami and Koutromanos, (2016).

Table **6**.1 Comparison between numerical values and experimental value.

Specimen	**Experimental value (Vu)**	**K&C (Vu)**	**Triaxial material mode (Vu)**	**Modified strut-and-tie model (Vu)**
C4G2	1658.5 KN	1665 KN	1655 KN	1666 KN

The results shown in Table 6.1 show that the triaxial material model has the closest value to the test, while the modified strut-and-tie model and the K&C material model have acceptable accuracy with a slight overestimation of the ultimate load.

CHAPTER SEVEN
CONCLUSIONS

In this study, the current version of the K&C material model was tested to assess its' accuracy in predicting UHPC behavior. The validation procedure is carried out by analyzing a single element made of UHPC using the auto generated parameters, and the analysis result was compared to the test result of a UHPC cube. The single element result shows that calibration of the K&C material model is required to predict UHPC behavior. The K&C material model was calibrated using a recently modified constitutive model developed specifically for UHPC. The three main groups of parameters of the K&C material modeled were calibrated according to the data obtained for a UHPC with a compressive strength of 150 MPa and the result of the calibrated parameters was validated by comparing it to a test data.

The triaxial material model proposed by Moharrami and Koutromanos (2016) consists of six lines of parameters. Each line is responsible of controlling a specific aspect of the concrete behavior. Some lines were straightforward like the first line, which contains the modulus of elasticity, shear modulus, and bulk modulus. The line responsible of the compressive behavior was calibrated using a cylinder specimen to match the result with the experimental data. The tensile behavior is controlled by multiple lines (tension and fiber parameters), and they were calibrated using a direct tensile test from the literature. It has been noted that this material model is superior in terms of capturing the effect of fiber's various effects on the analysis result. The triaxial material model offers the capability to adjust fibers characteristics like fibers length, diameter and mechanical properties according to the test result directly without having to adjust the constitutive laws like the K&C material model. Furthermore, fibers orientation is taken into consideration as the model simplifies the orientation of fibers into three main directions, which has been proven to heavily affect the analysis result. Fibers orientation parameters were calibrated using a proposed formula by El-Helou et al., (2020). Finally, the strain adjustment parameters were calibrated to predict the cracking formation within UHPC, which consists of multiple cracks at

different strain values. These strain values were taken from real test data and was is used by the material model to form the rotating smeared crack model.

The calibration of each material model is evaluated using single-element analysis, uniaxial cylinder compression, and direct tensile analysis, and the result is compared to the values collected from experiments. The calibrated material models were then utilized further to analyze a UHPC corbel specimen from the literature and assess the accuracy of the calibrated material models. The corbel was modeled as a half model utilizing the symmetry nature of the specimen. The concrete part was modeled using solid elements, and reinforcements were modeled using beam elements and it has shared nodes with the solid parts. The surface where the concentrated load is applied as well as the supports were modeled as elastic plates to avoid any local failure to concentrated load. The results obtained from the finite element analysis for both of the material models mentioned have excellent agreement with the test result, proving that the calibration procedure was successful.

Finally, a recently modified strut and tie model based on the truss method and specifically developed for UHPC corbel was investigated in this study. The STM takes into consideration the effect of main reinforcement, secondary reinforcement, and fiber forces. The proposed formulas were used to calculate the ultimate capacity of the same specimen analyzed by the two material models mentioned earlier, and the predicted value is in a good agreement with both the test result and the analysis.

The conclusions from this study are:

- The calibration procedure proposed by Xu and Wille (2014) for the K&C material model to analyze UHPC structural elements is reliable in providing the UHPC parameters.
- The UHPC corbel analyzed using the K&C material model in this study has acceptable accuracy compared to the test result.
- The calibration procedure of the triaxial material model proposed by Moharrami and Koutromanos (2016) is significantly easier than the K&C material model, requiring only uniaxial compression tests, direct tensile

tests, and calibrating the modified strain parameters of fibers to match the tensile stress-strain curve of the UHPC.

- The triaxial material model is more reliable in capturing the various effects of fibers like crack bridging and fiber orientation within the cementitious matrix due to the utilization of the fiber-modified strain and fiber orientation parameters, providing an acceptable accuracy in predicting the complete tensile behavior of the UHPC (hardening and softening behavior).
- The finite element analysis of the UHPC corbel utilizing the triaxial material model provided more accurate results than the K&C material model.
- The calibration of the K&C material model using the methodology proposed by Xu and Wille (2014) requires extensive work and trials, while calibrating the triaxial material model is significantly more straightforward, and changing one characteristic of the UHPC does not require calibration of the entire material model's parameters.
- The modified strut-and-tie model investigated in this study is used to predict the ultimate shear capacity of a UHPC corbel specimen. The model successfully provided a value that nearly matches the value obtained from the test.
- The suggestion for future studies is to investigate the effect of various parameters of UHPC corbels like the main tension reinforcement, secondary reinforcement, fiber volume, and UHPC properties on the behavior of the UHPC corbel using the material model investigated in this study.

REFERENCES

Abakumov, A. I., Safronov, I. I., Smirnov, A. S., Dyanov, D. Y., & Medvedkina, M. V. (2023). "A MODIFIED MODEL OF KARAGOZIAN & CASE CONCRETE IN LOGOS SOFTWARE PACKAGE." Problems of Strength and Plasticity.

Al-Quraishi, H. A., Mohamme, J. H., & Nada, S. S., (2018). "A New Shear Strength Model for UHPC Corbel." International Review of Civil Engineering (IRECE) 9, no. 4 (July 31, 2018): 168. https://doi.org/10.15866/irece.v9i4.14868.

Binici, B. (2005). "An Analytical Model for Stress–Strain Behavior of Confined Concrete." Engineering Structures 27, no. 7 (June 2005): 1040–51. https://doi.org/10.1016/j.engstruct.2005.03.002.

Candappa, D. C., Sanjayan, J. G., & Setunge S. (2001). "Complete Triaxial Stress-Strain Curves of High-Strength Concrete." Journal of Materials in Civil Engineering 13, no. 3 (June 2001): 209–15. https://doi.org/10.1061/(ASCE)0899-1561(2001)13:3(209).

Canha, R. M. F., Kuchma, D. A., El Debs, M. K., & De Souza, R. A. (2014). "Numerical Analysis of Reinforced High Strength Concrete Corbels." Engineering Structures 74 (September 2014): 130–44. https://doi.org/10.1016/j.engstruct.2014.05.014.

Drucker, D. C., and Prager, W. (1952). Soil mechanics and plasticity analysis or limit design. Quarterly of Applied Mathematics, 10: 157.

El-Helou, R. G., Koutromanos, I., Moen, C. D., & Moharrami M. (2020). "Triaxial Constitutive Law for Ultra-High-Performance Concrete and Other Fiber-Reinforced Cementitious Materials." Journal of Engineering Mechanics 146, no. 7 (July 2020): 04020062. https://doi.org/10.1061/(ASCE)EM.1943-7889.0001777.

Elzainy, A., Gırgın, S. G., and Yalçınkaya, C. (2023). "Numerical Investigation of a Concrete Material Model for Ultra-High Performance Concrete." In Proceedings of the 3rd International Civil Engineering & Architecture Conference Volume 1:

Civil Engineering. Golden Light Publishing, 2023. https://doi.org/10.31462/icearc.2023.sme534.

Erzar, B., Pontiroli, C., & Buzaud, E. (2016). “Shock Characterization of an Ultra-High Strength Concrete.” The European Physical Journal Special Topics 225, no. 2 (April 2016): 355–61. https://doi.org/10.1140/epjst/e2016-02637-4.

Fawaz, G., & Murcia-Delso, J. (2021). “Three-Dimensional Finite Element Modeling of RC Columns Subjected to Cyclic Lateral Loading.” Engineering Structures 239 (July 2021): 112291. https://doi.org/10.1016/j.engstruct.2021.112291.

Feng, S., Xiao, H., & Li, H. (2020). “Comparative Studies of the Effect of Ultra high-Performance Concrete and Normal Concrete as Repair Materials on Interfacial Bond Properties and Microstructure.” Engineering Structures 222 (November 2020): 111122. https://doi.org/10.1016/j.engstruct.2020.111122.

Green, B., Moser, D., Scott, D., & Long, W. (2015). “Ultra-High Performance Concrete History and Usage by the Corps of Engineers.” Advances in Civil Engineering Materials 4, no. 2 (July 30, 2015): 132–43. https://doi.org/10.1520/ACEM20140031.

Gee, D., Asaad, M., & Tadros, M. (2020). “Ultra-High-Performance Concrete Optimization of Double-Tee Bridge Beams.” The Concrete Bridge Magazine, 2020. https://www.aspirebridge.com/magazine/2020Winter/CBP-UHPC.pdf.

Helou, H. (2016). Multiscale Computational Framework for Analysis and Design of Ultra-High Performance Concrete Structural Components and Systems.

He, X., Ke, K. Guo, L., Yam, M., & Wang, Z. (2021). “A Replaceable Fuse Steel-Concrete Composite Connection: Force Transfer Mechanism and Design Considerations.” Journal of Constructional Steel Research 183 (August 2021): 106760. https://doi.org/10.1016/j.jcsr.2021.106760.

Yuan, H., Xia, W., & Hong, Z. (2024). “Shear Behavior of Ultra-High Performance Concrete corbels : Experimental Study and Modified Strut-and-Tie Model.”

Engineering Structures 310 (2024). https://doi.org/https://doi.org/10.1016/j.engstruct.2024.118043.

Xie, J., Elwi, A. E., & MacGregor, J. G., “Mechanical Properties of Three High-Strength Concretes Containing Silica Fume.” ACI Materials Journal 92, no. 2 (1995). https://doi.org/10.14359/9764.

Kalliontzis, D., & Salah, A. (2024). "Material Characterization of Ultra-High-Performance Concrete (UHPC)", in Database for Material Characterization of Ultra-High-Performance Concrete (UHPC). DesignSafe-CI. https://doi.org/10.17603/ds2-7gar-ps40

Kang, H., Willam, K., Shing, B., & Spacone, E. (2000). “Failure Analysis of R/C Columns Using a Triaxial Concrete Model.” Computers & Structures 77, no. 5 (July 2000): 423–40. https://doi.org/10.1016/S0045-7949(00)00006-7.

Kassem, W. (2015). “Strength Prediction of Corbels Using Strut-and-Tie Model Analysis.” International Journal of Concrete Structures and Materials 9, no. 2 (June 2015): 255–66. https://doi.org/10.1007/s40069-015-0102-y.

Kravanja, G., Mumtaz, A. R., & Kravanja, S. (2024). “A Comprehensive Review of the Advances, Manufacturing, Properties, Innovations, Environmental Impact and Applications of Ultra-High-Performance Concrete(Uhpc).” Buildings 14, no. 2 (February 1, 2024): 382. https://doi.org/10.3390/buildings14020382.

Lee, J., & Fenves, G. (1998) “Plastic-Damage Model for Cyclic Loading of Concrete Structures.” Journal of Engineering Mechanics 124, no. 8 (August 1998): 892–900. https://doi.org/10.1061/(ASCE)0733-9399(1998)124:8(892).

Lee, M., & Park, G. (2023). “Investigation of Constitutive Models of HPFRCC Subjected to Static and Dynamic Loadings.” Composite Structures 324 (November 2023): 117525. https://doi.org/10.1016/j.compstruct.2023.117525.

Leu, L., Huang, C., Chen, C., & Liao, Y. (2006). “Strut-and-Tie Design Methodology for Three-Dimensional Reinforced Concrete Structures.” Journal of Structural

Engineering 132, no. 6 (June 2006): 929–38. https://doi.org/10.1061/(ASCE)0733-9445(2006)132:6(929).

Magallanes, J., Wu, Y., Malvar, L., & Crawford, J. (2010). “Recent Improvements to Release III of the K&C Concrete Model.” 11th International LS-DYNA Users Conference 1, no. 3 (June 6, 2010): 37–48. https://lsdyna.ansys.com/wp-content/uploads/attachments/Simulation-1-4.pdf.

Malvar, L., Crawford, J., Wesevich, J., & Simons, D. (1997). “A Plasticity Concrete Material Model for DYNA3D.” International Journal of Impact Engineering 19, no. 9–10 (October 1997): 847–73. https://doi.org/10.1016/S0734-743X(97)00023-7.

Mander, J. B., Priestley, M. J. N., & Park, R. (1988). “Theoretical Stress-Strain Model for Confined Concrete.” Journal of Structural Engineering 114, no. 8 (September 1988): 1804–26. https://doi.org/10.1061/(ASCE)0733-9445(1988)114:8(1804).

Mirmiran, A., & Shahawy, M. (1997). “Dilation Characteristics of Confined Concrete.” Mechanics of Cohesive-Frictional Materials 2, no. 3 (July 1997): 237–49. https://doi.org/10.1002/(SICI)1099-1484(199707)2:3<237::AID-CFM32>3.0.CO;2-2.

Moharrami, M., & Koutromanos, I. (2016). “Triaxial Constitutive Model for Concrete under Cyclic Loading.” Journal of Structural Engineering 142, no. 7 (July 2016): 04016039. https://doi.org/10.1061/(ASCE)ST.1943-541X.0001491.

Attard, M. M., & Setunge, S. (1996). Stress-Strain Relationship of Confined and Unconfined Concrete, ACI Mater. J. (1996) 93. httpsdoi.org10.143599847.

Nguyen, D., Thai, D., Nguyen, H. T., Nguyen, T., & Le-Trung, K. (2021). “Responses of Composite Beams with High-Performance Fiber-Reinforced Concrete.” Construction and Building Materials 270 (February 2021): 121814. https://doi.org/10.1016/j.conbuildmat.2020.121814.

Panjehpour, M., Ali, A. A. A, Parvez, A. M., Aznieta, F. N., & Voo, Y. L. (2012). “An Overview of Strut-and-Tie Model and Its Common Challenges.” International

Journal of Engineering Research in Africa 8 (December 2012): 37–45. https://doi.org/10.4028/www.scientific.net/JERA.8.37.

Popovics, S. (1973). "A Numerical Approach to the Complete Stress-Strain Curve of Concrete." Cement and Concrete Research 3, no. 5 (September 1973): 583–99. https://doi.org/10.1016/0008-8846(73)90096-3.

Ridha, M. M. S., Al-Shafi'i, N. T. H., & Hasan, M. M. (2017). "Ultra-High Performance Steel Fibers Concrete Corbels: Experimental Investigation." Case Studies in Construction Materials 7 (December 2017): 180–90. https://doi.org/10.1016/j.cscm.2017.07.004.

Saatcioglu, M., & Razvi, S. R. (1992). "Strength and Ductility of Confined Concrete." Journal of Structural Engineering 118, no. 6 (June 1992): 1590–1607. https://doi.org/10.1061/(ASCE)0733-9445(1992)118:6(1590).

Samani, A., & Attard, M. M. (2012). "A Stress–Strain Model for Uniaxial and Confined Concrete under Compression." Engineering Structures 41 (August 2012): 335–49. https://doi.org/10.1016/j.engstruct.2012.03.027.

Sohail, M. G., Kahraman, R., Al Nuaimi, N., Gencturk, B., & Alnahhal, W. (2021). "Durability Characteristics of High and Ultra-High Performance Concretes." Journal of Building Engineering 33 (January 2021): 101669. https://doi.org/10.1016/j.jobe.2020.101669.

Su, Q., Wu, H., & Fang, Q. (2022). "Calibration of KCC Model for UHPC under Impact and Blast Loadings." Cement and Concrete Composites 127 (March 2022): 104401. https://doi.org/10.1016/j.cemconcomp.2021.104401.

Tadros, M. K., Gee, D., Asaad, M., & Lawler, J. (2020). "Ultra-High-Performance Concrete: A Game Changer in the Precast Concrete Industry." PCI Journal 65, no. 3 (2020). https://doi.org/10.15554/pcij65.3-06.

Teng, J., Xiang, Y., Yu, T., & Fang, Z. (2019). "Development and Mechanical Behaviour of Ultra-High-Performance Seawater Sea-Sand Concrete." Advances in

Structural Engineering 22, no. 14 (October 2019): 3100–3120. https://doi.org/10.1177/1369433219858291.

Thai, D., & Nguyen, D. (2020). “Calibrating the K&C Material Model for Fiber Reinforced Concrete Structures.” In: Reddy, J., Wang, C., Luong, V., Le, A. (eds) ICSCEA 2019. Lecture Notes in Civil Engineering, vol 80. Springer, Singapore. https://doi.org/10.1007/978-981-15-5144-4_19

Teng, J., Xiang, Y., Yu, T., & Fang, Z. (2019). “Development and Mechanical Behaviour of Ultra-High-Performance Seawater Sea-Sand Concrete.” Advances in Structural Engineering 22, no. 14 (October 2019): 3100–3120. https://doi.org/10.1177/1369433219858291.

Wang, Y., Wang, Y., Zhao, Y., Li, G., Lyu, Y., & Li, H. (2020). “Experimental Study on Ultra-High Performance Concrete under Triaxial Compression.” Construction and Building Materials 263 (December 2020): 120225. https://doi.org/10.1016/j.conbuildmat.2020.120225.

Williams, E. M., Graham, S. S., Akers, S. A., Reed, P. A., & Rushing, T. S. (2010). “Constitutive Property Behavior of an Ultra-High-Performance Concrete with and without Steel Fibers.” Computers and Concrete 7, no. 2 (April 25, 2010): 191–202. https://doi.org/10.12989/CAC.2010.7.2.191.

Wu, J., Li, J., Du, X., & Liu, X. (2017). “Numerical Study on the Asphalt Concrete Structure for Blast and Impact Load Using the Karagozian and Case Concrete Model.” Applied Sciences 7, no. 2 (February 17, 2017): 202. https://doi.org/10.3390/app7020202.

Wu, Y., Crawford, J., Lan, S., & Magallanes, J. M. (2014). “Validation Studies for Concrete Constitutive Models with Blast Test Data.” (2014).

Xiao, Q. G., Teng, J. G., & Yu, T. (2010). “Behavior and Modeling of Confined High-Strength Concrete.” Journal of Composites for Construction 14, no. 3 (June 2010): 249–59. https://doi.org/10.1061/(ASCE)CC.1943-5614.0000070.

Xu, M., & Wille, K. (2014). “Calibration of K&c Concrete Model for Uhpc in Ls-Dyna.” Advanced Materials Research 1081 (December 2014): 254–59. https://doi.org/10.4028/www.scientific.net/AMR.1081.254.

Xu, S., Wu, P., & Wu, C. (2020). “Calibration of KCC Concrete Model for UHPC against Low-Velocity Impact.” International Journal of Impact Engineering 144 (October 2020): 103648. https://doi.org/10.1016/j.ijimpeng.2020.103648.

Yaşayanlar, Y. (2023). “Material Model Calibration of Fiber Reinforced Concrete Using Deep Neural Network.” Izmir Institute of Technology, 2023. https://hdl.handle.net/11147/13951.

Yasser, M. (2022). “Numerical Modeling of UHPC Using a Concrete Damage Plasticity Model.” University of Nevada, 2022.

Yin, X., Li, Q., Xu, X., Chen, B., Guo, K., & Xu, S. (2023). “Investigation of Continuous Surface Cap Model (CSCM) for Numerical Simulation of Strain-Hardening Fibre-Reinforced Cementitious Composites against Low-Velocity Impacts.” Composite Structures 304 (January 2023): 116424. https://doi.org/10.1016/j.compstruct.2022.116424.

Zhang, N., Tan, K., & Leong, C. (2009). “Single-Span Deep Beams Subjected to Unsymmetrical Loads.” Journal of Structural Engineering 135, no. 3 (March 2009): 239–52. https://doi.org/10.1061/(ASCE)0733-9445(2009)135:3(239).

Zhang, S. S., Wang, J. J., Yu, G., & Fernando, D. (2023). “Stress-Strain Models for Ultra-High Performance Concrete (Uhpc) and Ultra-High Performance Fiber-Reinforced Concrete (Uhpfrc) under Triaxial Compression.” Construction and Building Materials 370 (March 2023): 130658. https://doi.org/10.1016/j.conbuildmat.2023.130658.